EXPERIMENTAL INVESTIGATION OF THE RELATIONSHIP BETWEEN FINITE ELEMENT MODELING AND DIGITAL IMAGE CORRELATION

by

Nicole Nmair

A Thesis
Submitted to the
Graduate Faculty
of
George Mason University
in Partial Fulfillment of
The Requirements for the Degree
of
Master of Science
Civil and Infrastructure Engineering

Committee:

_____	Dr. David Lattanzi, Thesis Director
_____	Dr. Girum Urgessa, Committee Member
_____	Dr. Viviana Maggioni, Committee Member
_____	Dr. Ossama Salem, Department Chair
_____	Dr. Kenneth S. Ball, Dean, Volgenau School of Engineering
Date: _____	Fall Semester 2018 George Mason University Fairfax, VA

Experimental Investigation of the Relationship Between Finite Element Modeling and Digital Image Correlation

A Thesis submitted in partial fulfillment of the requirements for the degree of Master of Science at George Mason University

by

Nicole Nmair
Bachelor of Science
George Mason University, 2016

Director: David Lattanzi, Assistant Professor
Sid and Reva Dewberry Department of Civil, Environmental, and Infrastructure Engineering

Fall Semester 2018
George Mason University
Fairfax, VA

ACKNOWLEDGEMENTS

I would like to thank my family and friends for their continued support and encouragement through my pursuit of higher education. I would also like to thank Dr. David Lattanzi for his mentorship in the development of this research. In addition, thank you to my committee and the George Mason University Civil and Infrastructure Engineering Department for giving me the opportunity to present my research.

TABLE OF CONTENTS

LIST OF TABLES

LIST OF FIGURES

LIST OF EQUATIONS

LIST OF ABBREVIATIONS AND SYMBOLS

Analysis Systems Inc…….…… ANSYS
Applied Force……..F
Area of Interest……..... AOI
Coefficient of Determination……...……. R^2
Deflection Along the Beam.....……δ(x)
Derived Strain Along the Beam for Load 1.....…….. $\varepsilon(x)_1$
Derived Strain Along the Beam for Load 2.....…….. $\varepsilon(x)_2$
Derived Strain Along the Beam for Load 3.....…….. $\varepsilon(x)_3$
Digital Image Correlation ……...…….. DIC
Digital Image Correlation Deflection at a Distance x…...…...……..… $\delta(x)_{DIC}$
Distance Along the Beam ……...x
Distance from the Neutral Axis of the Beam…….…..y
Field of View ……FOV
Finite Element……..…… FE
Finite Element Deflection at a Distance x……..…… $\delta(x)_{FE}$
Finite Element Model Updating..……..…… FEMU
Frequency Response Function……....FRF
Inch……in
Integrated Digital Image Correlation….……IDIC
Kilogram ……...kg
Length of Beam ……..L
Megapixel ……....MP
Modulus of Elasticity……..……... E
Moment ……...…… M(x)
Moment of Inertia ……... I
Pound-force……...lbf
Pound per Square Inch……..psi
Second Derivative of Deflection……δ"(x)
Strain……... ε(x)
Stress…….....σ(x)

ABSTRACT

EXPERIMENTAL INVESTIGATION OF THE RELATIONSHIP BETWEEN FINITE ELEMENT MODELING AND DIGITAL IMAGE CORRELATION

Nicole Nmair, M.S.

George Mason University, 2018

Thesis Director: Dr. David Lattanzi

This thesis investigates the comparison between the behavior of a structure modeled in a finite element (FE) software to the behavior captured using Digital Image Correlation (DIC). This experiment opens the gateway to quicker and easier structural assessments of the nation's infrastructure through the use of DIC, a research area that requires further investigation. Through experimental analysis, the ability of DIC to be used as a finite element calibration tool was tested. Comparisons were completed by analyzing and comparing the behavior of a fixed-fixed aluminum frame under varying static loads at the midspan of the beam. Two structural parameters were assessed in the comparative analysis including the structures response strain and deflection. Through the analysis of the deflection, an adequate comparison was concluded between DIC and the FE model, with average absolute differences in deflection between 0.004866 and 0.007075 inches. However, the structures strain response consisted of high error in the DIC strains resulting in unsuccessful comparisons between DIC and the FE model. These errors are predicted to

have been caused by vibration in the system during loading, noise caused by high light reflectivity, construction error, and primarily, speckle pattern inadequacy. Since the deflection results were deemed feasible, Euler-Bernoulli theory was used to derive strain equations from DIC deflections, resulting in viable strain results for the structure. Overall, DIC's ability to be used as a finite element model updating tool was confirmed yet requires further investigation into optimization methods for model parameter updating. Through this research, a better understanding of the limitations of the DIC was investigated, providing recommendations on the method of initial calibration between DIC and FE software.

CHAPTER 1: INTRODUCTION

1.1. Motivation

As the nation's infrastructure continues to degrade under increasing user demand, new structure assessment methods must be introduced to aid in structural health monitoring. Structural health monitoring is defined as the identification, inspection, testing, data acquisition, analysis, and evaluation of a structure's condition through routine inspections and testing (Gul 2009). Structural health monitoring requires the use of reliable technology to make assessment decisions. According to the American Society of Civil Engineers, the United States contains approximately 614,387 bridges which require continuous inspection and maintenance ("Bridges" 2017). Inspections of structures are needed to determine the system's reactions and behaviors to changing loads such as evolving traffic demands. Using new technology such as digital image correlation (DIC), may provide a quick way to capture full field measurements to determine structural behavior.

DIC is a non-contact optical measurement method that captures full field displacement and strain of a structure via image analysis of pattern deformations (Wang et al. 2011b). This method has been increasingly used as a tool to assess a structure's deformation. Through strain and displacement measurements, DIC has been used on various material specimens subjected to different load states to determine deformation. In

addition, DIC has been used to compute a structure's mechanical properties. For example, parameters such as modulus of elasticity and thermal expansion coefficients have been identified through estimation techniques (Pan et al. 2009). Research into DIC's ability as a calibration tool for finite element model updating is minimally studied.

Through the application of DIC, a finite element (FE) model may be developed and updated to replicate current structural conditions to aid assessment of structures. Having the ability to correlate real structure behavior to a FE model opens the door for structural health monitoring and finite element model updating (FEMU). To develop such models, initial calibration must be performed to ensure model accuracy and relationship to the real structure. Understanding the different components and limitations of DIC's ability to predict boundary conditions, material behavior, and structural behavior is pivotal in determining its use in structural inspections. Ultimately, DIC provides the opportunity to improve structural health monitoring systems.

1.2. Purpose of the Research

The purpose of this research is to evaluate the possibility of using DIC as a basic finite element model updating tool. The feasibility of correlating DIC to FE models to provide basic calibration is tested by comparing a structure's strain and deflection response under static loads. Understanding the system's limitations and the method of comparison allows for the calibration between DIC and FE models, to further research in the implementation of DIC on a larger scale structures.

1.3. Thesis Organization

This thesis is organized into a total of six chapters and an appendix. The first chapter presents an overview of the performed research and identifies the motivation of the research. Chapter 2 presents a literature review and expresses the need for this research in the structural engineering community. Chapter 3 delineates the means to use DIC and finite element software to test basic calibration of a structure. Furthermore, Chapter 4 characterizes the frame system tested and the FE model developed to test initial calibration. Moreover, the derived analytical equations are presented in this chapter to provide preliminary assessment of the viability of the outputted FE and DIC results. Strain and displacement results from DIC, the FE model, and the analytical equations are further analyzed and discussed in Chapter 5. In addition, Chapter 6 concludes the outcomes of this research including recommendations to this field of research. Lastly, the appendices present all DIC, FE model, and analytical data generated for this experimental investigation which were presented in Chapters 4 and 5.

CHAPTER 2: LITERATURE REVIEW

2.1. Introduction to Digital Image Correlation

Digital Image Correlation (DIC) is an optical-based tool that was first developed in the 1980s by researchers at the University of South Carolina (Pan et al. 2009). DIC provides full field measurements of several mechanical deformation parameters through pattern recognition and image analysis. Using a high-speed camera, pixel movement is tracked between images to extrapolate global strain and deflection along the structure. Furthermore, DIC is not only applicable in the civil engineering industry but the aerospace, automotive, and biological industries as well ("Correlated Solutions - Applications" n.d.).

The DIC process is broken into three main components as outlined in Figure 1.1. The three components include the preparation of the specimen, capturing reference and test images, and using computer programs to extract full field measurements of the specimen.

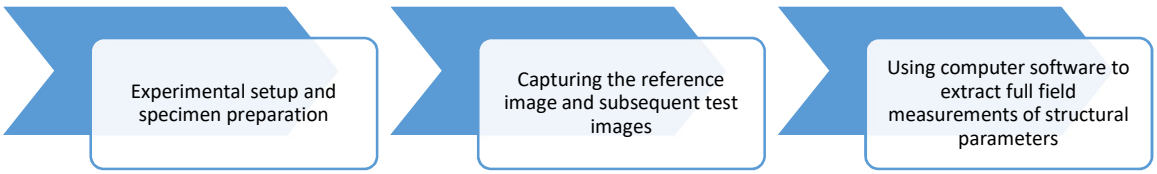

Figure 1.1. The DIC Process

The experimental setup and specimen preparation includes the construction of the specimen and the application of the speckle pattern to the specimen. The speckle pattern is a user applied set of dots that are sized according to the area of interest which provides the camera with tracking points. The applied speckle pattern plays the most significant role in result accuracy ("Application Note AN-1701 Speckle Pattern Fundamentals" n.d.). The DIC system includes the specimen of interest, a high-speed camera, a loading system, and a computer. An example of this setup is depicted in Figure 1.2.

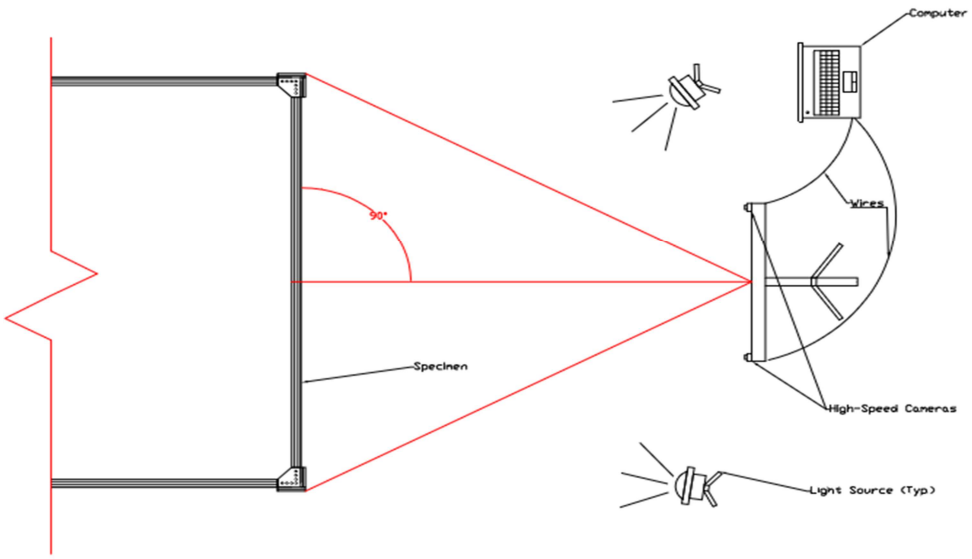

Figure 1.2. DIC Experimental Setup

The reference image is defined as the initial and un-deformed image of the specimen (Pan et al. 2009). The specimen is photographed in an inert state with no applied external loading. Next, the test image is captured after static loads have been applied to the system. Using computing software, full field measurements are extracted from pixel movement.

DIC captures initial states of pixels from the reference image and tracks pixel movement across the specimen surface in the test images to develop and quantify displacement and deformation across the specimen. DIC compares the reference image and the test image to extrapolate results using computer processing.

It should be noted that the DIC method has several limitations. The accuracy of the DIC method is dependent on the user's ability to provide a random speckle pattern across

the specimen and the quality of the captured images (Pan et al. 2009). DIC has primarily been used to capture structural deformation, and minimal research has been completed in DIC's use as finite element updating tool.

2.2. Previous FE Model Updating Methods

A finite element model is characterized as a two-dimensional (2D) or three-dimensional (3D) model that is representative of a real-life structure's geometric and material properties. A detailed FE model provides the potential for structure damage assessment, load rating, and prediction of a structure's remaining life (Garcia-Palencia et al. 2015). In order to match the structure closely, the FE model must be calibrated to reflect the structure's true response. This process is known as finite element model updating (FEMU). FEMU uses experimental measurements matched to finite element results of a structure's response for comparison. Model calibration seeks to reduce the differences between these two sets of results often by changing intrinsic properties of the structure. In order to update the model, a variety of calibration techniques have been researched, including the frequency response functions (FRF) method, time series analysis, and the use of strain gages.

Previous researchers have used frequency response functions to correlate structures to FE models of these structures. FRF is a two-step vibration-based method that uses frequency response functions and modal information of the structure to determine changes in structural parameters under dynamic loading. Parameters estimated include the stiffness, mass and boundary conditions of the structure. Garcia-Palencia et al. (2015) used FRF to

update an FE model of an in-service short span bridge. In addition, Zhang and Aktan (1997) developed an FE model of a Ohio bridge which was updated using the FRF method.

The advantage of using the FRF technique is its ability to capture differences in the stiffness, mass, and damping properties of the structure. This in turn provides the user with an ability to assess a structure's damage. This method requires a mathematical function to correlate the results detected analytically and experimentally which provides the user a method of updating the FE model. However, this method has several disadvantages including extraction errors, measurement errors, and structure inconsistencies. This method, unlike DIC is based on dynamic loading and relies on a structure's frequency and modal analysis.

Another FEMU technique that was investigated was the time series analysis method. This methodology seeks to use outputted ambient vibration data to detect a structure's damage. Damage locations and severity are identified providing important information regarding a structure's condition. Gul and Catbas (2011) employed this method on a steel structure. In their experiment, a steel frame was constructed, and an accompanying time series model was created. Different damage cases, such as varying boundary conditions and beam stiffness, were simulated. Vibration data was extracted from the frame by applying dynamic loads to the structure under these conditions. Using accelerometers, ambient vibration data was captured. Using random decrements, pseudo-free response data was derived, and a time series model was created for each sensor. Based on the healthy structure data extracted from the real structure and the time series model, damage was identified. The identification and location of the damage was completed using

differences between fit ratios. An advantage of using this method is that it only requires the healthy structure data. Therefore, damage conditions of the model are not required for analysis as the method predicts the response of the damaged system by using the undamaged structure data. However, the quantification of the damage was not achieved using this method.

Sanayei and Saletnik (1996) sought to develop a method for parameter estimation of a structure using strain gages. This method, like DIC, can be used to identify structural response under static loads to estimate structural damage and parameters. As a result of strain measurements, FE models are updated based on the parameter estimation. This process was performed on a 2D frame and a 2D truss. In addition, Sanayei et al. (2012) performed FE model updating in SAP2000, a structural software, using strain gage readings under controlled loading of a bridge. The initial model was updated manually based on measurements taken in the field on the structure. Throughout the experiment, the finite element model was refined by varying the material properties and geometrical properties. It was concluded that using a 3D FE model was feasible in modeling bridges with a high degree of accuracy. In addition, using strain data for FE model calibration was highly effective however, the placement and installation of gages proved to be inefficient. There are many other issues with using strain gages including noise, temperature effects, and placement errors.

Researchers Shafiei Dizaji et al. (2018) used DIC captured full field measurements combined with a hybrid genetic algorithm to update finite element models. Through the use of the captured DIC strain and deformation responses, an objective function was

established and refined until convergence between experiment and finite element model strains and displacements were achieved. In doing so, a foundation for DIC in structural identification was established. Tests were performed on a beam with varying loadings to identify parameters of the structure including the boundary conditions and material properties. Throughout the experiment, errors due to noise and limitations of the DIC were encountered.

2.3. Prior DIC Applications

DIC has been used in previous applications including the use of the I-DIC, Integrated Digital Image Correlation, method. This method is a two-stage coupled method encompassing DIC and mechanical identification processes. Leclerc et al. (2009) modeled structures using multiple finite elements for which polynomial basis functions were used. Multiple simulations were run and the FE models were updated based on a best fitting shape function. This correlation method requires a high degree of computer processing and is based on using cross-correlation functions to update FE models.

Moreover, Wang et al. (2011a) used DIC for full field measurements in updating a FE model of a composite panel. The correlation of the mode shapes and natural frequencies of the structure were used to parameterize the finite element model. Through investigation, boundary conditions and geometric portions of the panel were adjusted in the FE model. It was concluded that the best updating algorithm was through the comparison of natural frequencies and the mode shapes of the structure.

Previous researchers have sought to evaluate the possibility of using DIC for unmanned aerial structural health monitoring applications. In testing the ability to use DIC

in autonomous inspection, DIC's ability to be used in technology-based inspections was investigated. Reagan et al. (2018) concluded that using DIC on unmanned aerial vehicles did not majorly affect the precision of the DIC measurements. Therefore, DIC can improve structural health monitoring techniques for bridge assessments and inspections.

DIC has been used to capture full field measurements of different types of structures. For example, Baqersad et al. (2014) used DIC to extract full field measurements of a wind turbine blade. DIC strain and deformations compared well to typical wired measurement devices such as strain gages. In using DIC for wind turbine condition assessments, a better understanding of the blade's behavior was demonstrated. Furthermore, DIC has been used to assess the shear capacity of prestressed concrete beams. By using DIC, full field measurements were captured and analyzed as the prestressed beams were loaded. It was concluded that DIC provided a valuable technique in assessing the mechanical response of the prestressed beam with errors comparable to that of current numerical methods (De Wilder et al. 2015).

2.4. Summary of Literature Review

Several researchers have sought to correlate FE models to real specimens using field measurements. Researchers Zhang and Aktan (1997) and Garcia-Palencia et al. (2015) used frequency response functions to update FE models that were based on existing bridges. Furthermore, using time series analysis and ambient vibration data, structure damage responses were predicted by Gul and Cabtas (2011). In addition, through the use of strain measurements captured by strain gages, Sanayei and Saletnik (1996) and Sanayei et al. (2012) were able to update FE models. Wang et al. 2011 used DIC on a composite

panel and successfully updated the FE model based on the comparison of mode shapes and frequencies of the structure. Furthermore, Shafiei Dizaji et al. (2018) used DIC to identify material properties and boundary conditions of a beam for FEMU. Reagan et al. (2018) tested DIC in unmanned aerial vehicles with positive outcomes. Moreover, DIC has also been used by Baqersad et al. (2014) on wind turbine condition assessments. Lastly, De Wilder et al. (2015) tested DIC's ability to track prestressed concrete beam capacity measurements. While varying FEMU methods exist, minimal research has been done the use of DIC as a FEMU tool.

Unlike previous research, the scope of this research focuses on understanding the applicability of DIC to calibrate FE models, a gap that has been minimally studied. This thesis seeks to close this research gap through the correlation of DIC to FE models strains and deflections under controlled static loads. By understanding DIC's ability to detect deformations and strains, initial calibration between DIC and FE models can be done, opening the gateway to FEMU. Using DIC as a FEMU tool, provides a new technique to capture and use full field deformation measurements to the fullest extent.

CHAPTER 3: METHODOLOGY

The focus of this chapter is to discuss the general procedure of performing a comparison between DIC and FE strain and deflection measurements. This chapter discusses the three components needed including, the construction and testing of the frame using DIC, the development and testing of the replicated FE model, and the relationship between these two components to analytical results and each other.

A constructed frame is loaded and tested using DIC providing experimental measurements. An FE model is then designed in finite element software with matching intrinsic properties of the structure. Loading the FE model provides a second set of results for calibration. Furthermore, analytical results are used as preliminary checks to ensure basic structural behavior is followed. Model calibration is performed through the comparison of the DIC and FE model strain and deflection results. This general process is outlined in Figure 3.1.

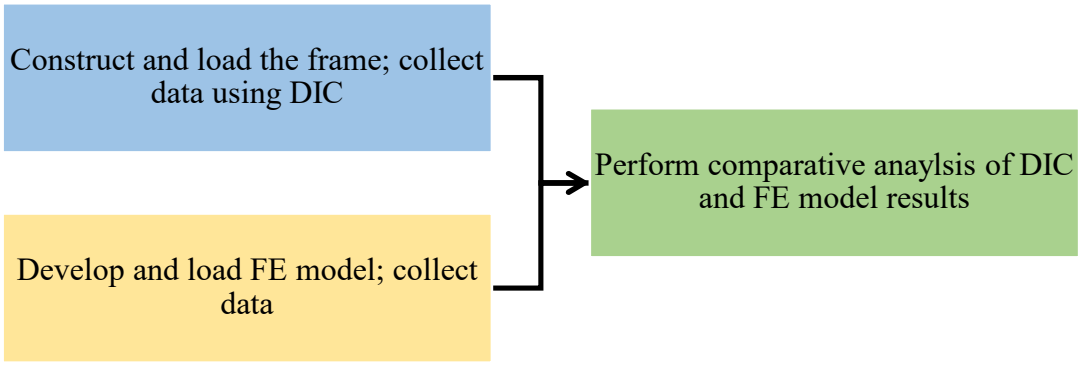

Figure 3.1. Generalized Updating Methodology

3.1. System Fabrication & Instrumentation

The first step is to identify the geometry and material properties of the frame that will be constructed. The structural properties that must be considered include frame geometry, constitutive properties of the frame, and the boundary conditions. After selecting geometric and material properties of the frame, the system is constructed with the selected connection points and supports. System construction begins with securing the frame columns firmly to the ground using anchors. After connecting the columns to the ground, connection to the horizontal frame components must be completed. Using plate connections, bolts, and L-shape stiffeners, firm connections may be accomplished. Once frame construction is complete, the DIC equipment must then be set up in accordance with manufacturer recommendations.

The DIC equipment includes a camera, calibration boards, a computer, and if needed, spotlights. DIC set up must be done to ensure the specimen is approximately in parallel with the plane of the pair of cameras. Spotlights may be set up to increase visibility of the specimen however, care must be taken to reduce high reflectively on the specimen surface. Once the frame is constructed, a speckle pattern must be selected and applied to the specimen.

3.1.1. Application and Selection of the Speckle Pattern

Based on the area of interest (AOI) and the quality of the camera used, a speckle pattern is chosen. The speckle pattern provides points that the DIC system will track to measure deformations. Therefore, it plays a pivotal role in the success and accuracy of the analysis. In order to have a successful speckle pattern, the AOI must satisfy the following criteria ("Application Note AN-1701 Speckle Pattern Fundamentals" n.d.):

- Achieve a 50% speckle coverage ratio.
- Attain a high contrast between the specimen and the applied speckle pattern
- Be comprised of consistent speckle sizes
- Accomplish a random speckle pattern with uniform and unbiased areas of speckle

The speckle coverage ratio is defined as the ratio of the area that is speckled to the area that is not speckled. According to the manufacturer, a 50% speckle coverage is recommended. Based on the speckle size, the distance between each speckle should be that of the speckle size. This, along with the speckle contrast, directly affects DIC's ability to track pixel movement.

A high color contrast between the specimen color and the color of the speckles is required. Therefore, using a black speckle pattern on a white specimen surface achieves the greatest contrast and is recommended. If the color contrast is not achieved with the specimen's current finishing, the frame may be spray painted using non-reflective paint prior to the application of the speckle pattern. In addition, spotlights may be used to assist with the brightness/contrast of the speckle pattern/frame. Furthermore, the speckle dot size and distribution play a key role in providing an adequate pattern.

The selection of the speckle dot size is dependent on the size of the field of view (FOV) and the camera resolution being used. As the camera resolution increases, the dot size decreases for a constant FOV due to its increased ability to capture pixels. If the pattern selected is too small, aliasing may occur. Aliasing is the camera's inability to accurately represent the specimen movements smoothly due to the camera's resolution being lower than the pattern sizing ("Application Note AN-1701 Speckle Pattern Fundamentals" n.d.). Table 3.1 outlines the varying dot sizes as recommend by the manufacturer.

Table 3.1. Speckle Dot Size ("Correlated Solutions – The DIC Speckle Kit" n.d.)

	Field of View					
	0.007" (0.18 mm) Dot Size	0.013" (0.33 mm) Dot Size	0.026" (0.66 mm) Dot Size	0.05" (1.27 mm) Dot Size	0.10" (2.54 mm) Dot Size	0.20" (5.08 mm) Dot Size
1 MP Camera 1024 pixels across	0.9" - 2.4" 2.3 cm - 6.1 cm	1.7" - 4.4" 4.2 cm - 11 cm	3.3" - 8.9" 8.4 cm - 23 cm	6.4" - 17.1" 16 cm - 43 cm	12.8" - 34.1" 33 cm - 87 cm	26.6" - 68.3" 65 cm - 173 cm
2.3 MP Camera 1920 pixels across	1.7" - 4.5" 4.3 cm - 11 cm	3.1" - 8.3" 7.9 cm - 21 cm	6.2" - 16.6" 16 cm - 42 cm	12.0" - 32.0" 31 cm - 81 cm	24.0" - 64.0" 61 cm - 163 cm	48.0" - 128.0" 122 cm - 325 cm
5 MP Camera 2448 pixels across	2.1" - 5.7" 5.4 cm - 15 cm	4.0" - 10.6" 10 cm - 27 cm	8.0" - 21.2" 20 cm - 54 cm	15.3" - 40.8" 39 cm - 103 cm	30.6" - 81.6" 78 cm - 207 cm	61.2" - 163.2" 155 cm - 415 cm
16 MP Camera 4872 pixels across	4.3" - 11.4" 11 cm - 29 cm	7.9" - 2 1.1" 20 cm - 54 cm	15.8" - 42.2" 40 cm - 107 cm	30.5" - 81.2" 77 cm - 206 cm	60.9" - 162.4" 155 cm - 413 cm	121.8" - 324.8" 309 cm - 825 cm

In addition, the speckle pattern distribution significantly affects the DIC's ability to track pixel movement. The spatial distribution must be random to reduce the probability of false matching. False matching is defined as DIC's inability to independently track a speckle's deformation due to its graphic similarity to nearby pixels. As a result, the pixel's movement is inaccurately tracked. Dot templates are recommended to reduce false matching. In addition, by using dot templates, the probability of having unbiased and uniform areas along the FOV is improved, increasing pattern adequacy ("Application Note AN-1701 Speckle Pattern Fundamentals" n.d.).

3.1.2. DIC Image Processing

Once the speckle pattern is applied to the structure, reference and test images are taken. Reference image accuracy plays a key role in determining the measurement of the loaded structure. Once reference images are taken, the system is loaded, and test images are taken. Test images are taken for every load that is applied while the reference image must only be captured once for each FOV. All images are run through VIC-3D, a DIC processing software. The software tracks pixel movement between the reference images and the test images, extracting parameters such as strain and deformation.

3.2. FE Model Development

Once the structural system is constructed, a 3D FE model is generated. The FE model should be built within a FE model software following the same geometry and material properties of the constructed system. The model must be created as a static

structural system and material assignments must be specified. Once geometry and material inputs are complete, assumptions for the boundary conditions are made.

3.3. Load Selection

Several loads large enough to induce measurable strain in the frame are then specified. Once loads are selected, experimental testing commences and results are extracted for calibration. These loads are inputted for FE analysis as well.

3.4. Calibration

Once strain and deflection results for both DIC and the FE model are collected, a comparison can be performed. An analysis is completed through the comparison of the DIC and FE deflection and strain results. An initial calibration check can be completed between the DIC and the analytical results as well as the FE model and the analytical results. Through this basic check, the magnitude and direction of the strain and deflection results are cross checked with the expected values.

Once preliminary checks between the DIC and FE model results to the analytical equations are performed, a comparison between the DIC and FE model is performed. A best fit line function is used to generate strain and deflection equations based on the DIC results. A comparison between the DIC best fit line and the FE model function can then be performed. The absolute difference and error between these two sets of data is calculated for defined points along the beam using the Equations (3-1) and (3-2):

$$Difference = |\delta(x)_{DIC} - \delta(x)_{FE}| \quad \text{Equation (3-1)}$$

$$\% \, error = \left| \frac{\delta(x)_{DIC} - \delta(x)_{FE}}{\delta(x)_{FE}} \right| * 100 \qquad \text{Equation (3-2)}$$

Based on the location of each measurement, a strain comparison is performed between the FE model results and that of DIC. This is completed by calculating the absolute difference between the two strain values at one defined distance along the beam using Equation (3-1). In addition, absolute percent errors are calculated for further comparison. By comparing strain and deflection values at defined points, an additional comparison between the two systems is completed.

CHAPTER 4: EXPERIMENTAL ANALYSIS

To test this approach, a series of tests were performed. First, a structural frame was constructed then, an accompanying FE model was developed for a singular component of the frame. Through the selection of a single horizontal frame component, beam behavior was initiated under static loading. In addition, analytical equations were derived for initial comparison to DIC and FE results. Once all three components were developed, loads were applied to the frame and results were captured using DIC. The same loads were then applied to the FE model and results were outputted for analysis.

Initial analysis was performed for both DIC and FE model results against analytical solutions. For DIC, a successful relationship was achieved for deflection however for strain large error was experiment which is further discussed in this chapter. With regards to the FE model, a successful comparison between the FE model and analytical solutions was achieved. Further comparisons between DIC and FE model was performed with the largest differences at the midspan.

4.1. General Properties of the Structural System

The structural frame constructed for these experiments consisted of four horizontal frame elements, referred to as beams, supported on columns. The beams, columns, and plate fasteners were made from aluminum grade 6105-T5 and were manufactured by 80/20 Inc. In addition, a load hanger connection device was milled and attached to the system

prior to loading. Figures 4.1 and 4.2 represent the plan and elevation views of the tested frame.

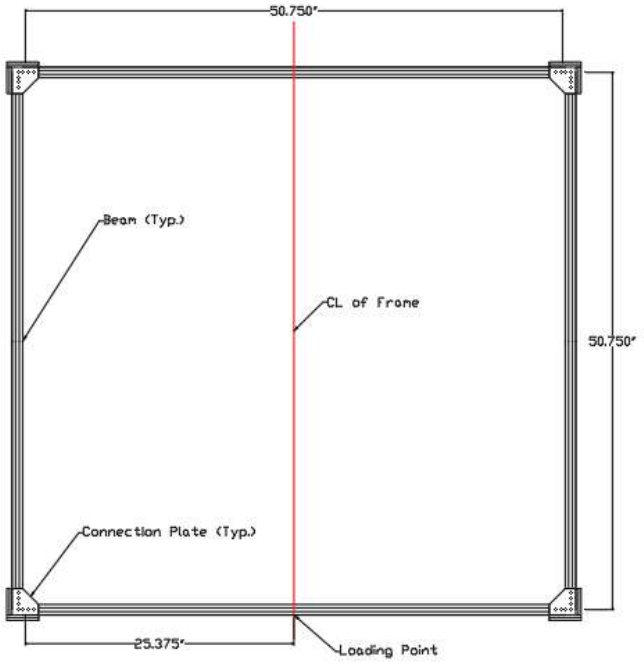

Figure 4.1. Plan View of the Frame

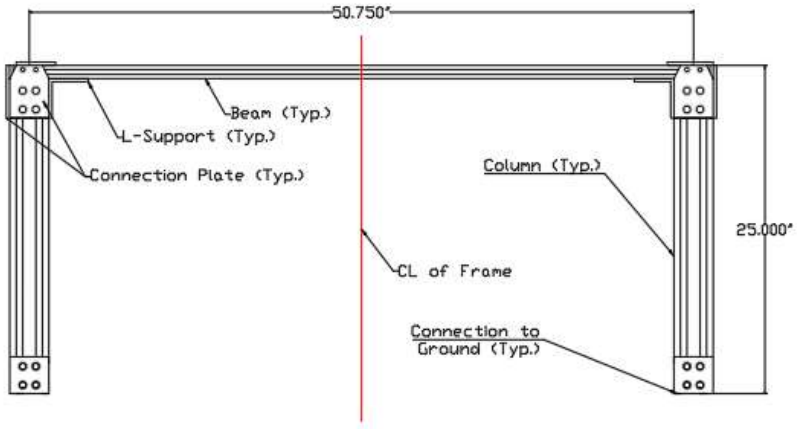

Figure 4.2. Elevation View of Frame

4.1.1. Properties of the Beam

For this experiment, a 54.5-inch long beam was selected as the system to be analyzed with a 50.75-inch column to column length. The beam was manufactured by 80/20 Inc., model 1010-S. The beam was fixed at both ends to the columns and consisted of a cross-sectional geometry as depicted in Figure 4.3.

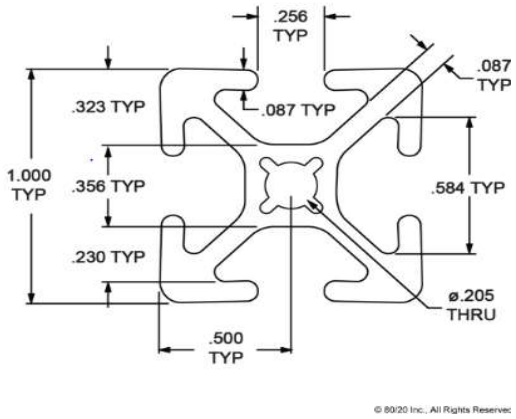

Figure 4.3. Cross Section of the Beam

In addition, Table 4.1 further outlines the geometrical and material properties as of the beam.

Table 4.1. Properties of the Beam

Beam Property	Value
Profile	Smooth Surface T-Slotted Profile
Material	Aluminum

Grade	6105-T5
Modulus of Elasticity	10,200,000 psi
Moment of Inertia	0.0463 in^4
Yield stress	35,000 psi
Height	1 in
Width	1 in
Weight	0.0424 lbf/in
Surface Area	0.437 in^2

4.1.2. Properties of the Columns

A total of four columns were used in the structural system. Similar to the beams, the columns were also manufactured by 80/20 Inc. of model 3030-S. Using columns and beams from the same manufacturer allowed for ease of connection and matching material properties. Figure 4.4 depicts the cross section of the columns used in the system.

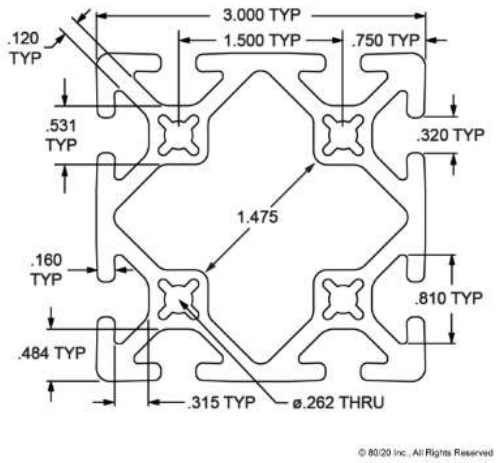

Figure 4.4. Cross Section of the Columns

Connections between beams and columns were completed using L-shaped stiffeners and steel gusset plates. Both connection devices were made of 6105-T5 aluminum and were affixed with black zinc bolts. The L-shape stiffeners acted as inside corner brackets, securing the bottom of the beam to the column, providing additional rigidity. In addition, a third bracket was used to secure two beams together on the inside face of the column. The gusset plates were used on both outer faces of each column and on the top face of the beams to secure the frame system together. A total of 3 gusset plates and 3 L-shaped stiffeners were used for each column totaling to 24 frame connection devices. A typical corner detail is provided in Figure 4.5.

Figure 4.5. Typical Column to Beam Connection

4.1.3. Properties of the Hanger Connection Device

In addition, an aluminum hanger connection device was milled to the fit the beam. A hanger device was required to hang load weights onto the beam. The geometry of the hanger connection device fitted the interior t-slotted geometry of the beam.

4.2. Speckle Pattern Selection & Application

Prior to applying the black speckle pattern, the beam was sprayed painted with a white spray paint. The type of spray paint used was compatible with ferrous and non-ferrous metals and sprays flat. The flat spray application reduced the reflectivity of light onto the camera when pictures were taken of the beam. A white paint was selected to provide the largest contrast to the black speckle pattern. This was done to meet the speckle contrast criteria. After the paint fully dried, using a speckle pattern roller, a black speckle

pattern was rolled onto the beam. For this experiment, a 5-megapixel (MP) camera was used with an AOI ranging between 8 and 21.2 inches. Therefore, a speckle pattern roller with a 0.026-inch dot size was used as depicted in Figure 4.6.

Figure 4.6. Speckle Pattern Ink Roller

After selecting and rolling the speckle pattern onto the beam, a visual inspection of the pattern was completed. In order to characterize a successful pattern, there must be a high contrast which is characterized as having a white background with black speckles. Secondly, a 50 percent ratio of speckled to not speckled areas on the beam was verified. In addition, a consistent speckle size must be used across the AOI. Once the speckle pattern was deemed acceptable, the DIC camera and spotlights were positioned.

4.3. Loading

A total of 7 preliminary weights, ranging between 3 to 33 kilogram (kg), were loaded onto the beam. Of these weights, three pertinent weights were selected for further

evaluation and are the results shown here. The three weights selected were chosen to provide the greatest strain and deflection ranges. Other results were similar. The three selected weights were hung onto the hanger connection device located 25.375 inches from the end of the beam at midspan. A 1 kg hanger, in conjunction with the hanger connection device, was used to hang the interlocking weights onto the beam. The three load cases were applied to the system in increasing order beginning with load one. The loads applied are identified in Table 4.2.

Table 4.2. Summary of Applied Loads

Load #	Weight (kg)	Weight (lbf)
1	8	17.64
2	18	39.68
3	33	72.75

4.4. DIC Equipment Setup and Imaging

The DIC equipment consisted of a pair of high speed cameras, two spotlights, a computer, and a standard calibration target board. In this experiment, the DIC equipment was set up twice to capture two FOVs. This resulted in a total of 182 images captured. These images included 110 calibration images, 12 reference images, and 60 test images for both FOVs for the three selected loads. Spotlights were used to indirectly light the beam

surface due to inadequate lighting in the room. A general layout of the equipment can be seen in Figure 4.7

.

Figure 4.7. General Layout of Equipment

4.4.1. Camera FOV

Two FOVs were of interest in this experiment. The first FOV captured 12.50 inches of the beam from the left support. The second FOV spanned from 12.50 inches from the left support to midspan of the beam. Both FOVs are depicted in Figure 4.8.

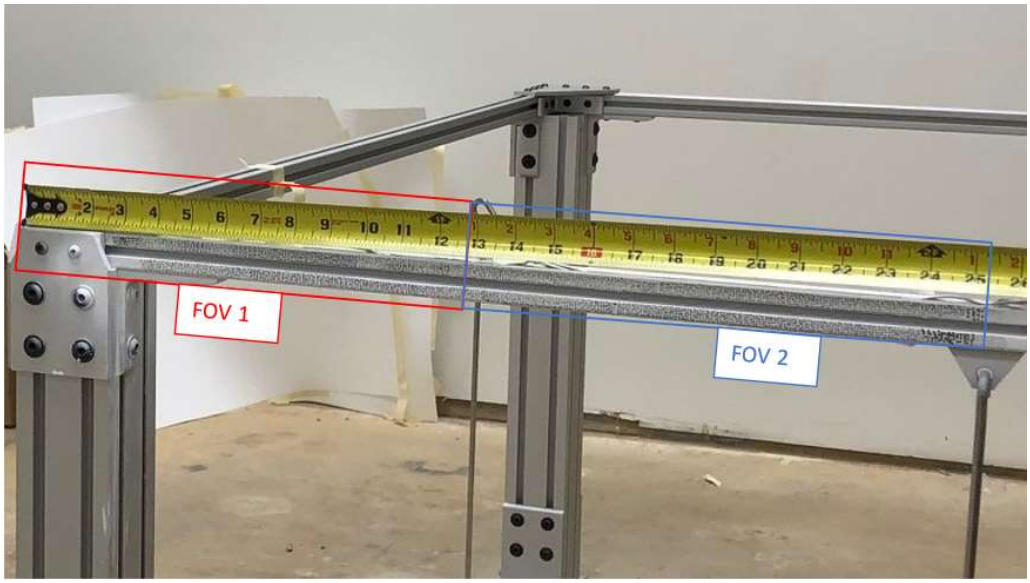

Figure 4.8. DIC Field of Views

A total length of approximately 25.50 inches was captured by combining both FOVs, encasing half the beam's length.

4.4.2. Calibration Imaging

Using the standard calibration target board, software-based calibration was performed in VIC 3D. This initial image calibration determines the cameras locations and captures the cameras intrinsic and extrinsic characteristics. In addition, this calibration removes lens distortions. In doing so, a 3D coordinate system was defined on the beam ("Correlated Solutions – Calibration" n.d.) In order to run the calibration, a total of 110 calibration images were taken for both field of views. In each image, the calibration board was placed in front of the specimen and rotated through different angles. These images

were then imported into VIC 3D and a calibration was run. Figures 4.9 and 4.10 represent examples of calibrations images used.

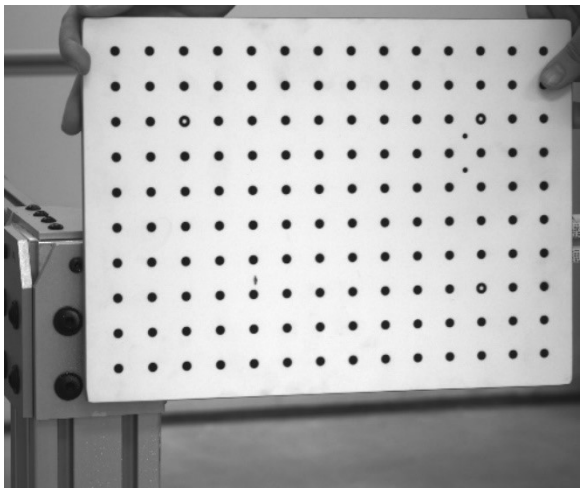

Figure 4.9. Calibration Image for FOV 1

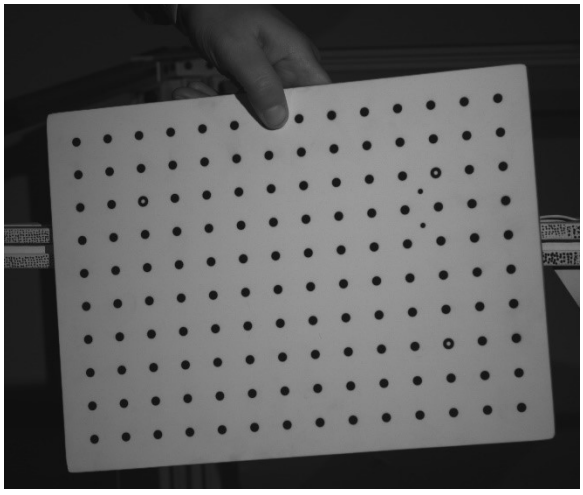

Figure 4.10. Calibration Image for FOV 2

Each FOV required its own set of calibration images and the calibration process was run independently.

4.4.3. Reference Imaging

Two sets of reference images were taken in this experiment. In the reference images, the beam was in the inert state with no applied loading. Each FOV required an independent set of reference images. Examples of the reference images are shown in Figures 4.11 and 4.12.

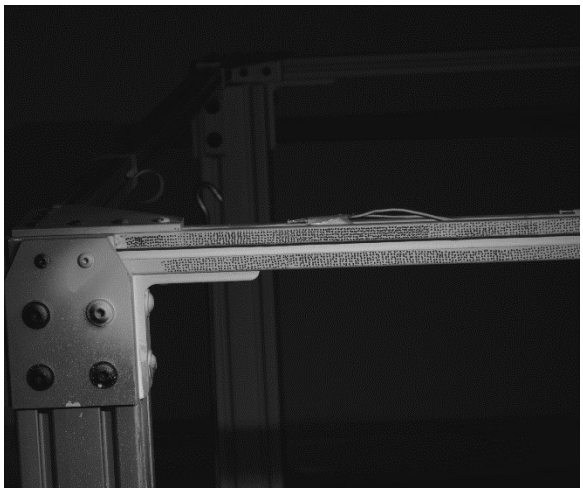

Figure 4.11. Reference Image for FOV 1

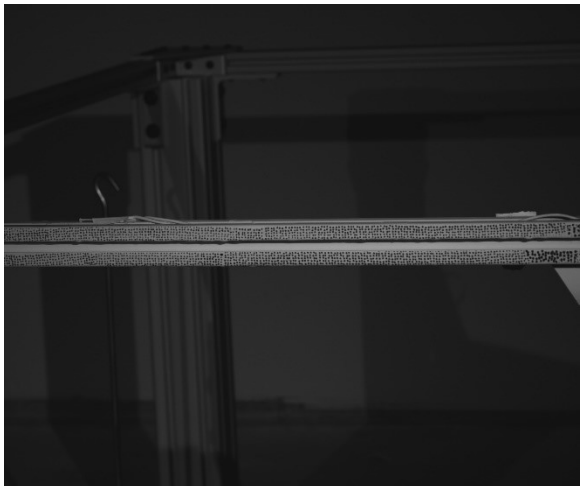

Figure 4.12. Reference Image for FOV 2

A total of 12 reference images were taken for both FOVs. After the images were taken, test imaging began.

4.4.4. Test Imaging

Once the reference images were captured, the test images were taken. The beam was loaded by placing the slotted weights on the hanger, located at the midspan of the beam. Once weights were loaded onto the system, time was taken to ensure the weights were not moving. Once the system was in the static state, 10 photos were taken for each load case. This process was repeated for every load for both FOVs, resulting in a total of 60 test images. Figures 4.13 and 4.14 represent two examples of test images for each FOV.

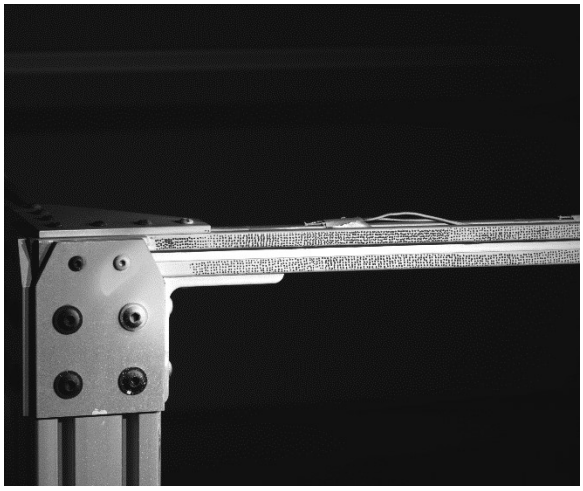

Figure 4.13. Test Image for FOV 1

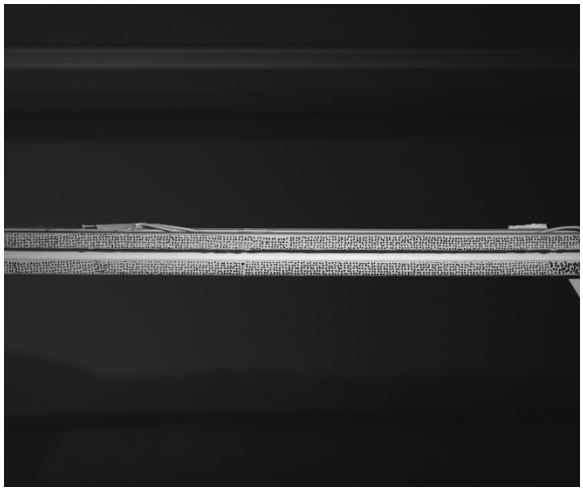

Figure 4.14. Test Image for FOV 2

4.4.5. Image Processing

After reference and test images were taken, they were imported into VIC-3D, a DIC specific program. An AOI was selected from the FOV and results were extracted along a

line. The AOI selected was the top flange of the beam for both FOVs. The AOI for FOV 1 spanned from 5.075 to 12.75 inches. Selection of this AOI within the DIC software is shown in Figure 4.15 for FOV 1. Furthermore, the AOI for FOV 2 spanned from 11.25 inches to midspan.

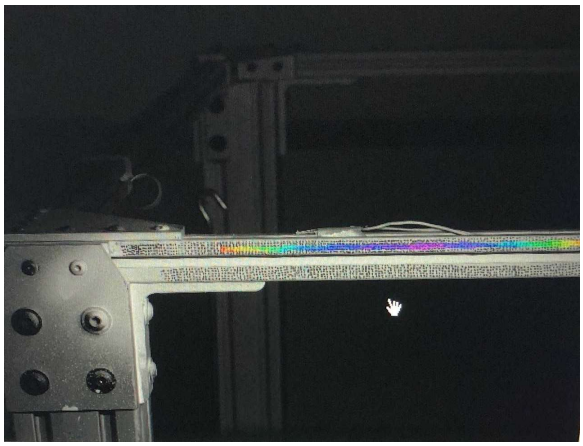

Figure 4.15. AOI Selection for FOV 1 in VIC 3D

4.5. FE Model

After the construction of the beam was completed, a FE model was developed. ANSYS version 19.2 was used for this experiment as the FE program of choice. A 3D rendering of the beam was developed to match the structure in the inert state. Both material and geometric properties were matched as closely as possible to the real structure.

4.5.1. Material Properties

Table 4.3 compares the material properties between the FE model and beam. The modulus of elasticity, yield stress, and moment inertias matched between the two systems.

Table 4.3. FE Model Material Assignment

Description	FE Model Input
Material	Aluminum
Modulus of Elasticity	10,200,000 psi
Yield Stress	35,000 psi

4.5.2. Geometry, Mesh Size, and Boundary Conditions

The 3D model matched the real structure's beam cross sectional properties and length. This was completed by projecting the online 80/20 Inc. model to the desired length of 50.75 inches in AutoCAD, a drafting software. This drawing was then imported into ANSYS version 19.2 as two 25.375-inch beam components. Once the geometry was imported, boundary conditions were applied to the beam. Several assumptions were made regarding the beam's boundary conditions. It was assumed that connections between the columns and beams were rigid and that the column was significantly stiffer than the beam. Therefore, it was assumed that under static loading, no rotational movement in the x, y, and z direction was experienced. As a result, the ends of the horizontal components were modeled as fixed supports and pure beam action was assumed. Mesh sizing was specified

for a minimum of 1 inch. By selecting a 1-inch mesh size, computing time was reduced and results were generated for every inch of the beam. Figures 4.16 presents the FE model layout. In this figure, the location of the fixed supports is shown as well as the location of the applied force. Furthermore, Figure 4.17 represents the meshing and general appearance of the FE model.

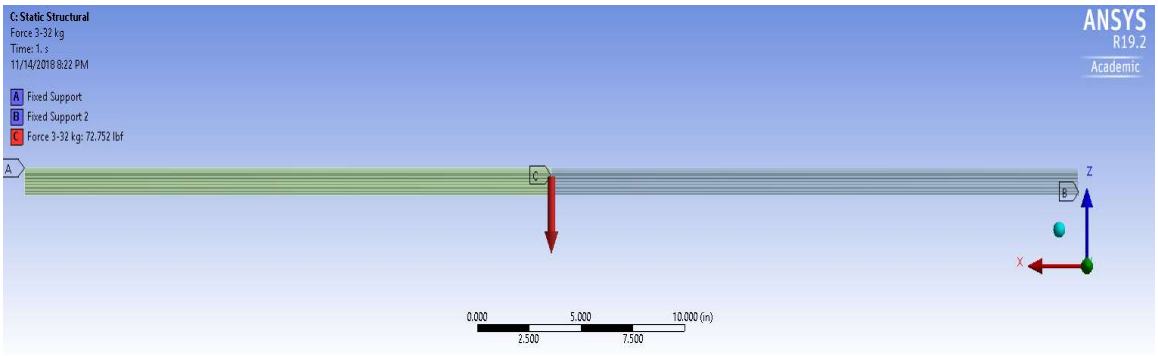

Figure 4.16. FE Model Layout

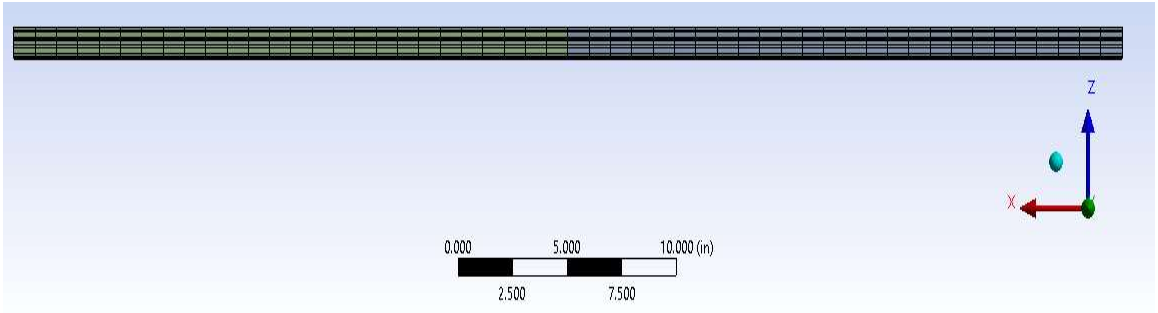

Figure 4.17. FE Model Mesh

4.5.3. Placement and Value of Loads

All loads were inputted into the FE model. The magnitudes of these forces were as shown in Table 4.2. For each test, the force was applied on the inside center edge of the beam, 25.375 inches from the beam ends, in the -Z direction.

4.5.4. AOI Results Output

As previously selected in the DIC program, the top flange of the beam was selected as the AOI in the FE model. Two structural outputs were generated for this AOI. This included the strain and the total deformation. The ANSYS output results are provided in Appendix C.

4.6. Analytical Equations

To verify that the FE model was performing correctly and to eliminate user error, a comparison to the analytical equation of Euler-Bernoulli strain and deflection was performed. By performing a comparison between the DIC and FE model results to that of the analytical results, a basic check was completed to ensure beam behavior occurred. Through the derivation of the fundamental relationship between stress and strain, a strain equation was developed for the fixed-fixed beam. While the system was a frame, the selection of the single horizontal frame component, the type of boundary conditions, and the placement of loading initiated beam behavior. Equation (4-1) defined stress as a function of the moment and geometric properties of the beam. Equation (4-2) represented Hooke's Law, the governing stress-strain relationship. By reordering the stress-strain

relationship in Equation (4-2), Equation (4-3) was developed for strain as a function of stress and the modulus elasticity of the beam.

$$\sigma(x) = \frac{M(x)y}{I} \quad \text{Equation (4-1)}$$

$$\sigma(x) = \varepsilon(x)E \quad \text{Equation (4-2)}$$

$$\varepsilon(x) = \frac{\sigma(x)}{E} \quad \text{Equation (4-3)}$$

Substituting Equation (4-1) into Equation (4-3), the strain along the beam was defined in Equation (4-4).

$$\varepsilon(x) = \frac{\left(\frac{M(x)y}{I}\right)}{E} \quad \text{Equation (4-4)}$$

Based on a fixed-fixed beam with a concentrated point load at midspan, analytical equations for strain were generated. Equation (4-5) represented the moment as a function of the distance along the fixed-fixed beam. Through the application of the stress-strain

relationship noted in Equation (4-3), Equation (4-6) was developed. Equation (4-6) represented strain as a function of distance along a fixed-fixed beam.

$$M(x) = \frac{F(4x-L)}{8} \quad ; \quad (0 \leq x \leq \frac{L}{2}) \qquad \text{Equation (4-5)}$$

$$\varepsilon(x) = \frac{\left(\frac{M(x)y}{I}\right)}{E} \qquad \text{Equation (4-6)}$$

By combining Equations (4-5) and (4-6), Equation (4-7) was formed. Equation (4-7) represented strain as a function of distance along the beam. This equation was then used to determine the analytical strain in terms of the beams geometry and material properties.

$$\varepsilon(x) = \frac{\left(\frac{F(4x-L)y}{I}\right)}{E} \quad ; \quad (0 \leq x \leq \frac{L}{2}) \qquad \text{Equation (4-7)}$$

In addition to strain, deflection equations were derived for the structure based on boundary conditions. Equation (4-8) provided the deflection as a function of distance along

the beam. The beam deflection was dependent on the beam length, force applied, and beam material properties as outlined. Furthermore, this equation was dependent on the boundary conditions selected, which in this case was a fixed-fixed condition.

$$\delta(x) = \frac{Fx^2(3L-4x)}{48EI} \quad ; \quad (0 \leq x \leq \frac{L}{2}) \qquad \text{Equation (4-8)}$$

Lastly, Equation (4-9) displays the strain-deflection relationship, which was used to derive strain from the analytical deflection functions.

$$\varepsilon(x) = y * \delta''(x) \qquad \text{Equation (4-9)}$$

In conclusion, Equations (4-8) and (4-9) were used to generate expected strain and deflection values for the structure. Using these two equations, DIC and FE model deflection and strain results were checked. In addition, best fit lines of strain were derived from deflection functions. Ultimately, Equations (4-8) and (4-9) served as baseline functions of structure behavior and for comparison.

CHAPTER 5: RESULTS

This chapter provides a comparison between the strain and deflection results outputted from DIC, the FE model, and the analytical solutions. Due to the symmetry of the beam and load placement, comparisons were performed in the top flange for half of the beam length. This chapter discusses the relationship between and FE model train and deflection values along the beam.

5.1. Comparisons of Deflection Results

First, a comparison was performed between the FE model and the analytical values of deflections. The FE model deflection and that of the analytical compared well with absolute differences less than 0.002 inches along the beam. The average absolute percent errors between these two data sets were around 6%. Figures 5.1, 5.2, and 5.3 show the relationship between the FE model response and the expected deflection along the beam for all three load cases.

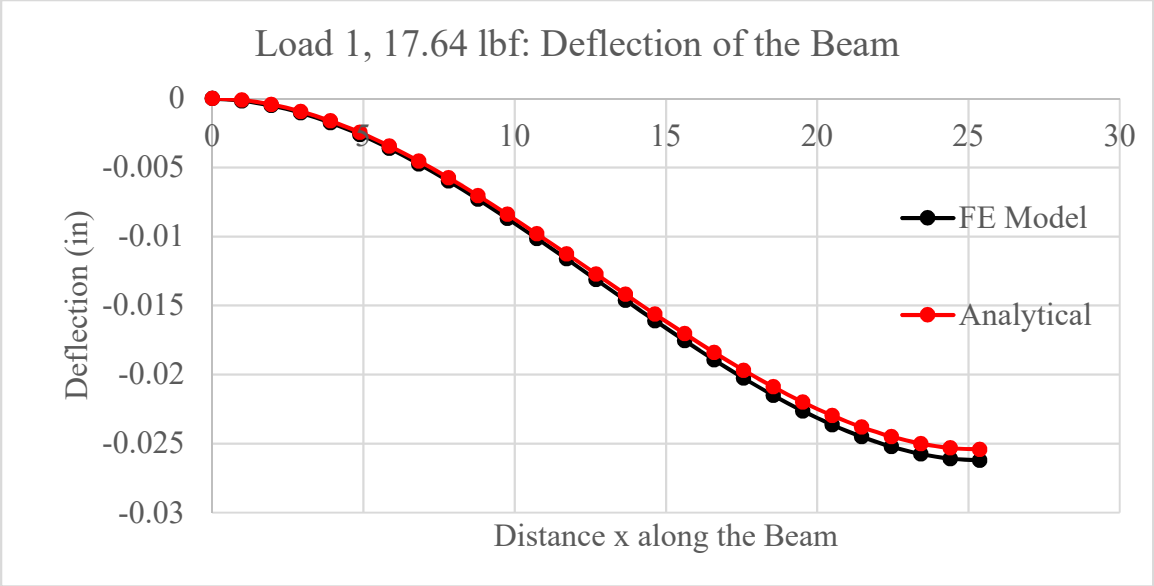

Figure 5.1. Load 1, 17.64 lbf: FE vs. Analytical Deflections

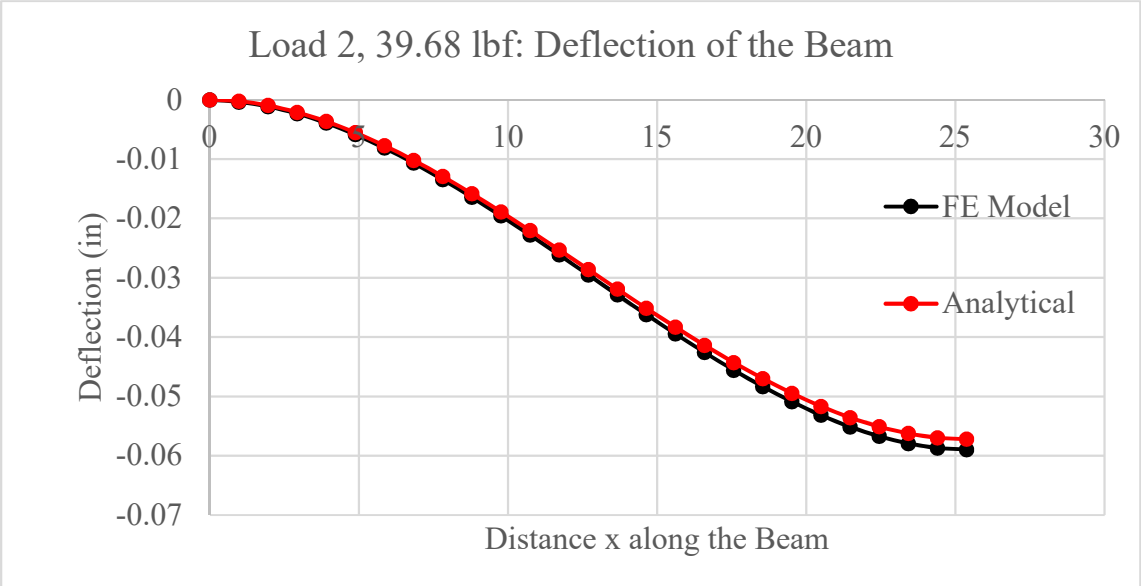

Figure 5.2. Load 2, 39.68 lbf: FE vs. Analytical Deflections

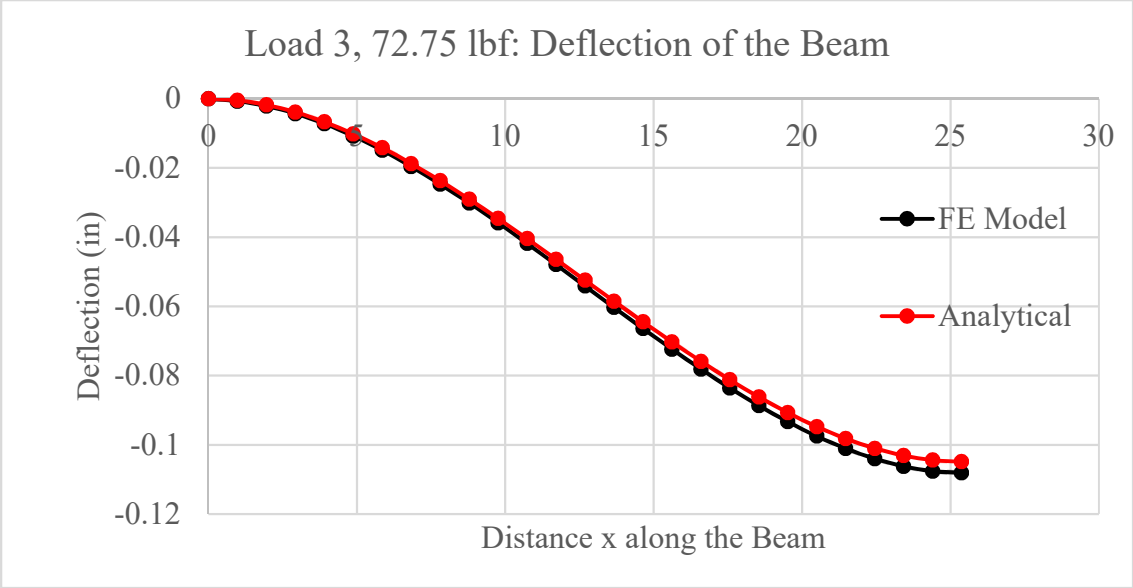

Figure 5.3. Load 3, 72.75 lbf: FE vs. Analytical Deflections

As the loading on the beam was increased, the differences between the FE model and the analytical deflections increased. The average absolute difference between the FE model and the analytical deflections was 0.000407, 0.000913, and 0.001674 inches. for loads 1, 2, and 3 respectively. The minimum, maximum, and average absolute percent errors between the FE model and the analytical deflections for load 1 were 3%, 35%, and 5% respectively. In addition, the minimum, maximum, and average absolute percent errors between the FE model and the analytical deflections for loads 2 and 3 were 0%, 53%, and 6% respectively. The minimum difference and error between these two systems was located at the fixed end of the beam. The location of the maximum difference across all loads was located near midspan. Overall, the comparison between the FE model and the analytical deflections was successful with small average absolute differences and percent errors.

Furthermore, DIC deflections were extracted and plotted for each load for both FOVs. By combining results from both FOVs, the entirety of the beams midspan was mapped. A line of best fit was performed in Excel as a third-degree polynomial for each load case with y-intercepts of zero. A third-degree polynomial was selected to match the order of the analytical equation presented in Equation (4-8). These results are shown in Figures 5.4, 5.5, and 5.6. Figure 5.4 depicts the line of best fit for Load 1. The R^2 coefficient of determination of the third-degree polynomial was 0.998, showing high correlation between the DIC values and the best fit line.

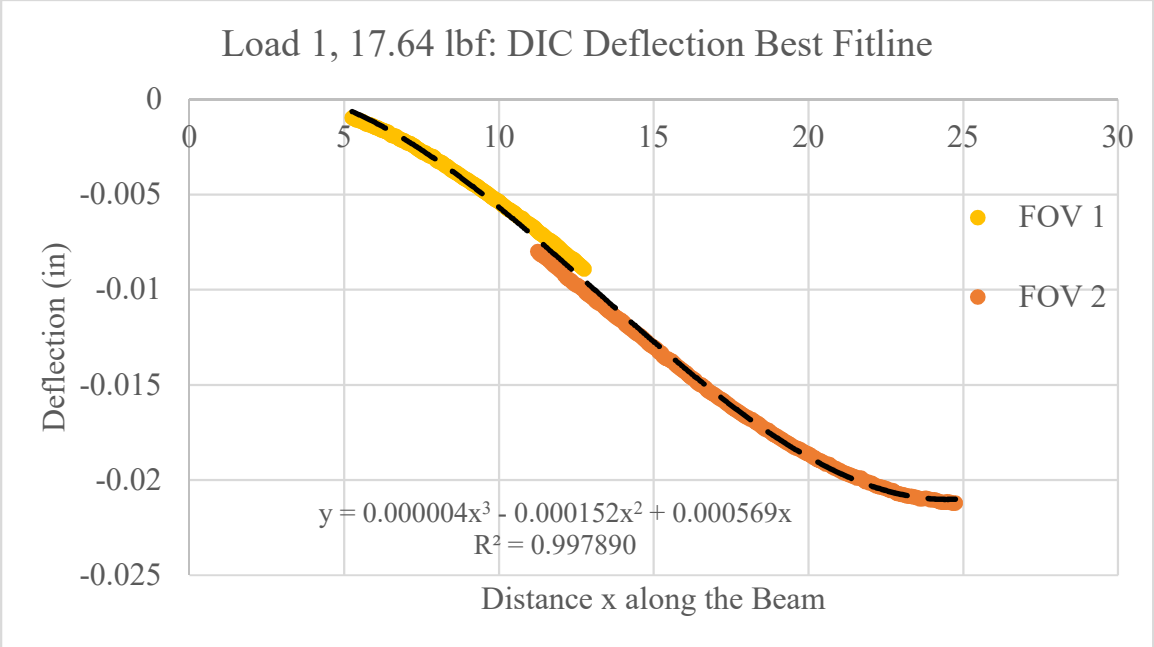

Figure 5.4. Load 1, 17.64lbf: DIC Deflection Best Fit Line

In addition, Figure 5.5 shows the best fit line for Load 2. As can be noticed, a third-degree polynomial with a high correlation was achieved.

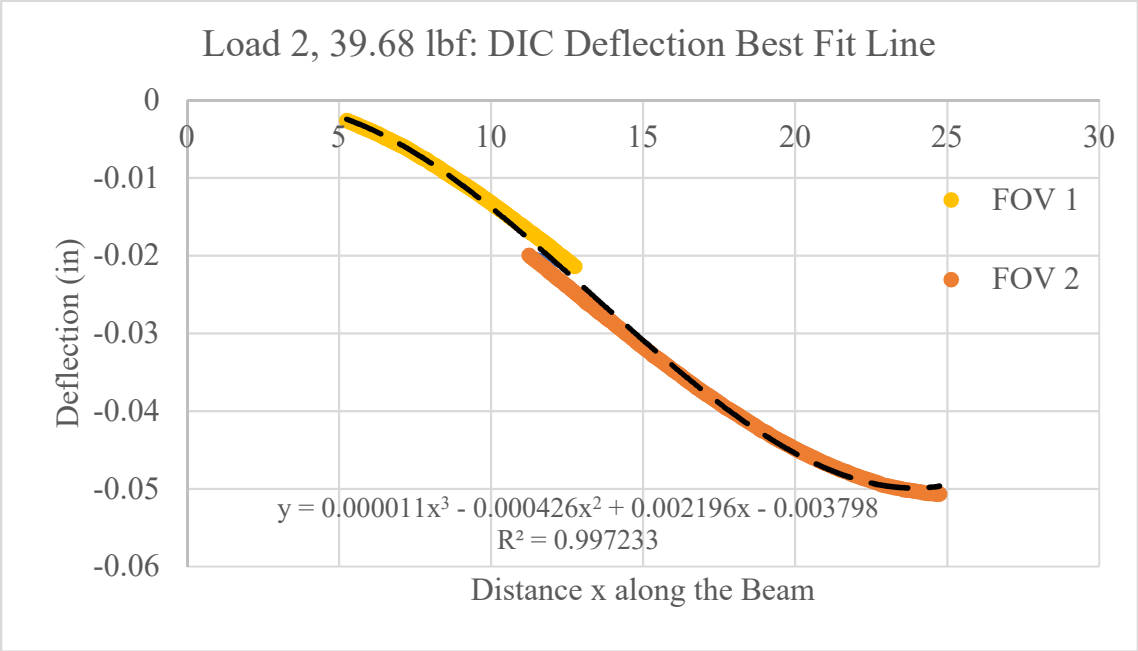

Figure 5.5. Load 2, 39.68 lbf: DIC Deflection Best Fit Line

Lastly, Figure 5.6 was generated for Load 3. Of all three load cases, this load case had the highest correlation of the best fit line.

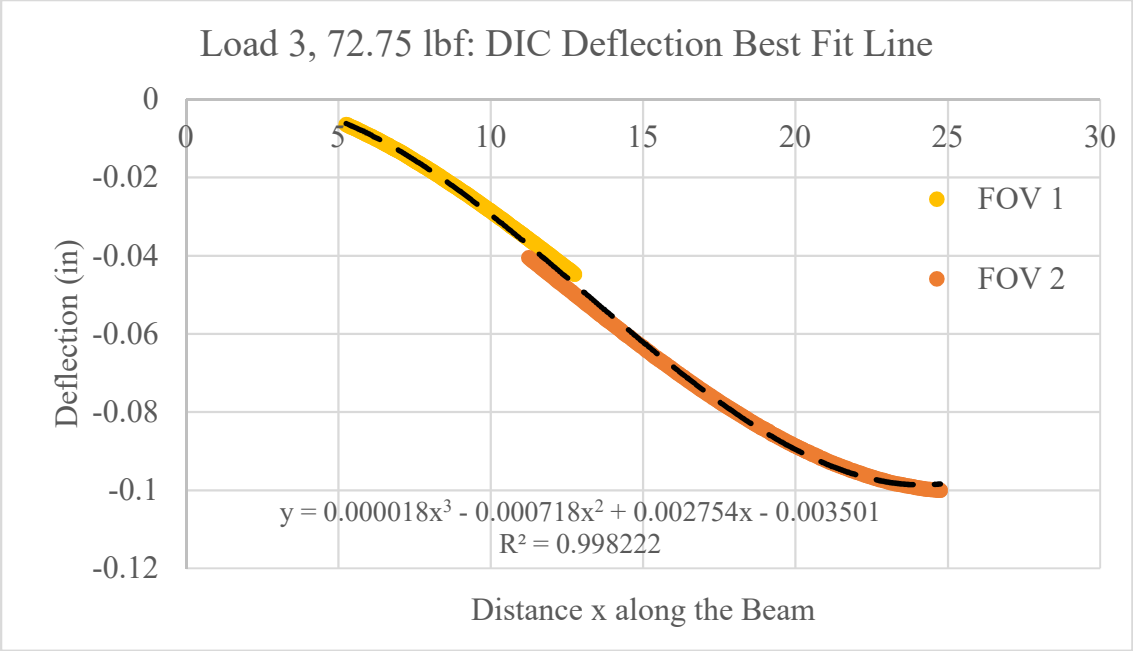

Figure 5.6. Load 3, 72.75 lbf: DIC Deflection Best Fit Line

Once best fit lines were generated for the DIC results, a comparison of these relationships to the analytical solutions was completed. This comparison was done to provide insight on the validity of the frame's assumed beam behavior. Figures 5.7, 5.8, and 5.9 display this relationship. The average difference between DIC and analytical deflections were 0.003603, 0.004107, and 0.00466 inches. for loads 1, 2 and 3 respectively. In addition, the average absolute percent error between DIC and analytical deflections for loads 1,2, and 3 were 32%, 19%, and 12%.

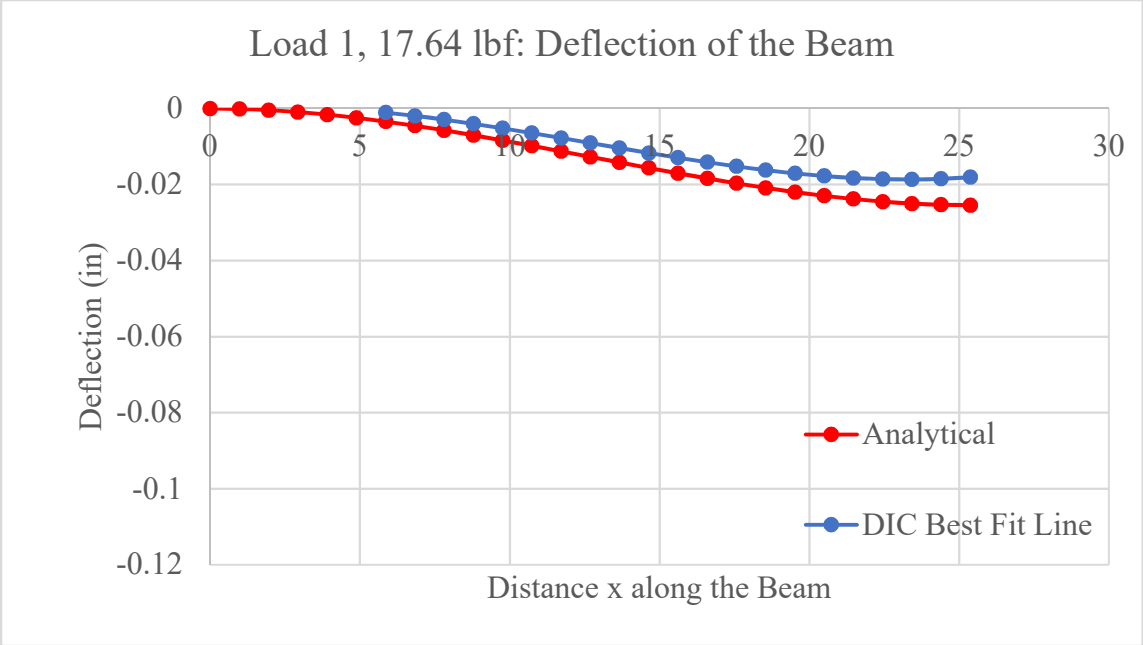

Figure 5.7. Load 1, 17.64 lbf: DIC Deflection Best Fit Line vs. Analytical Deflections

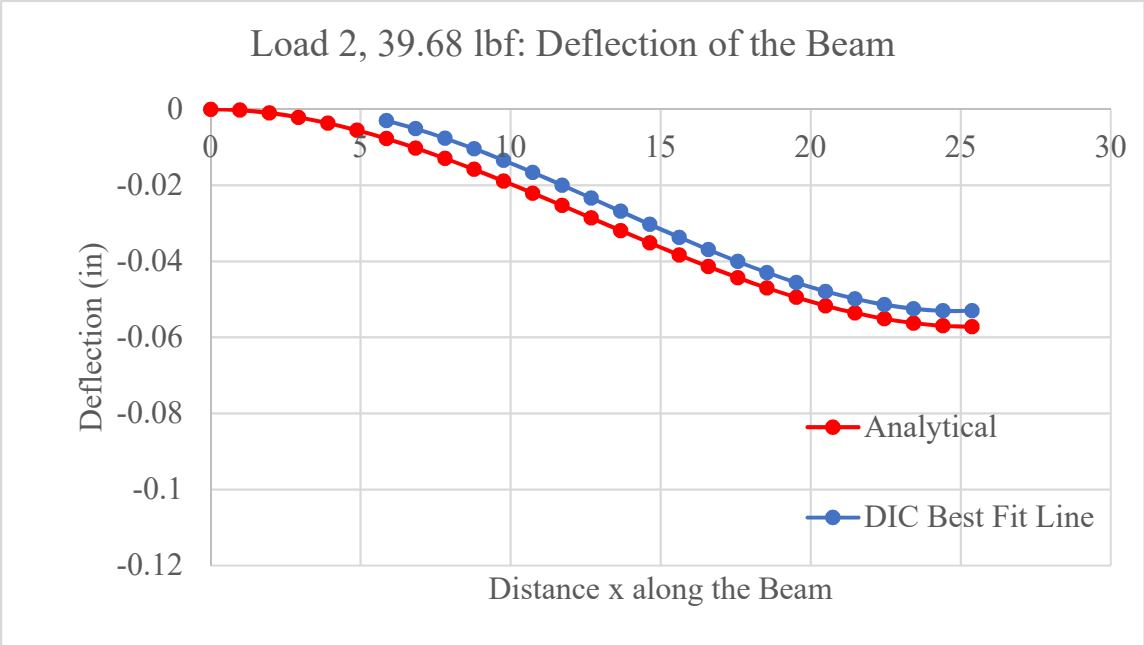

Figure 5.8. Load 2, 39.68 lbf: DIC Deflection Best Fit Line vs. Analytical Deflections

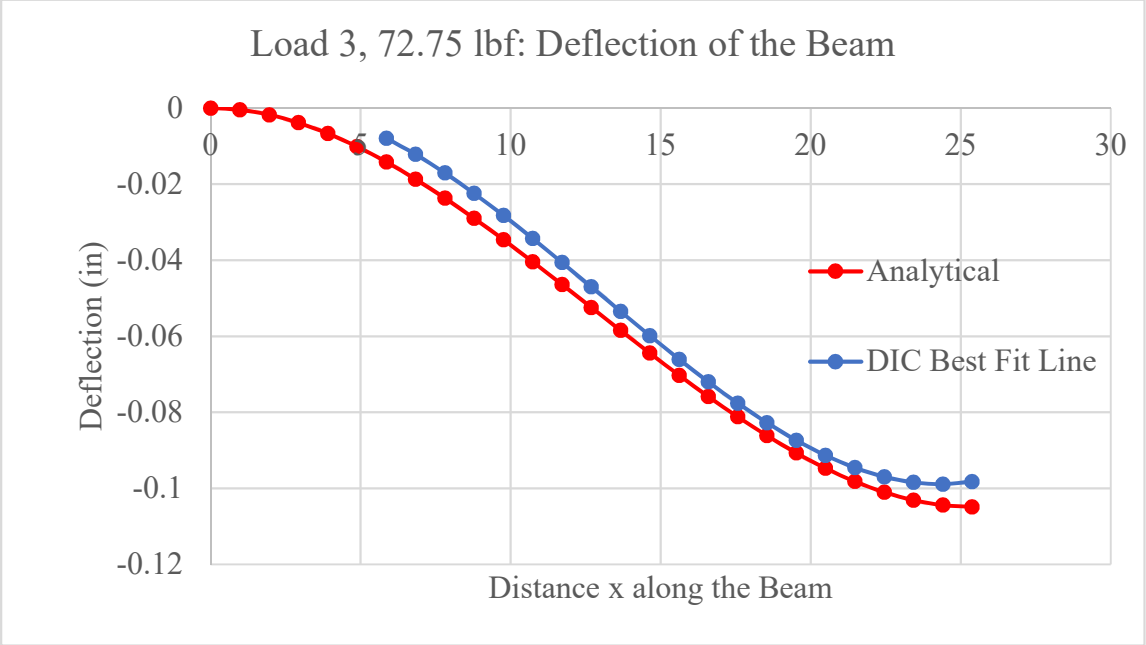

Figure 5.9. Load 3, 72.75 lbf: DIC Deflection Best Fit Line vs. Analytical Deflections

In order to fully understand the relationship between the FE model and the DIC deflection, results were graphed. Figures 5.10, 5.11 and 5.12 show the relationship between the two sets of results of deflection.

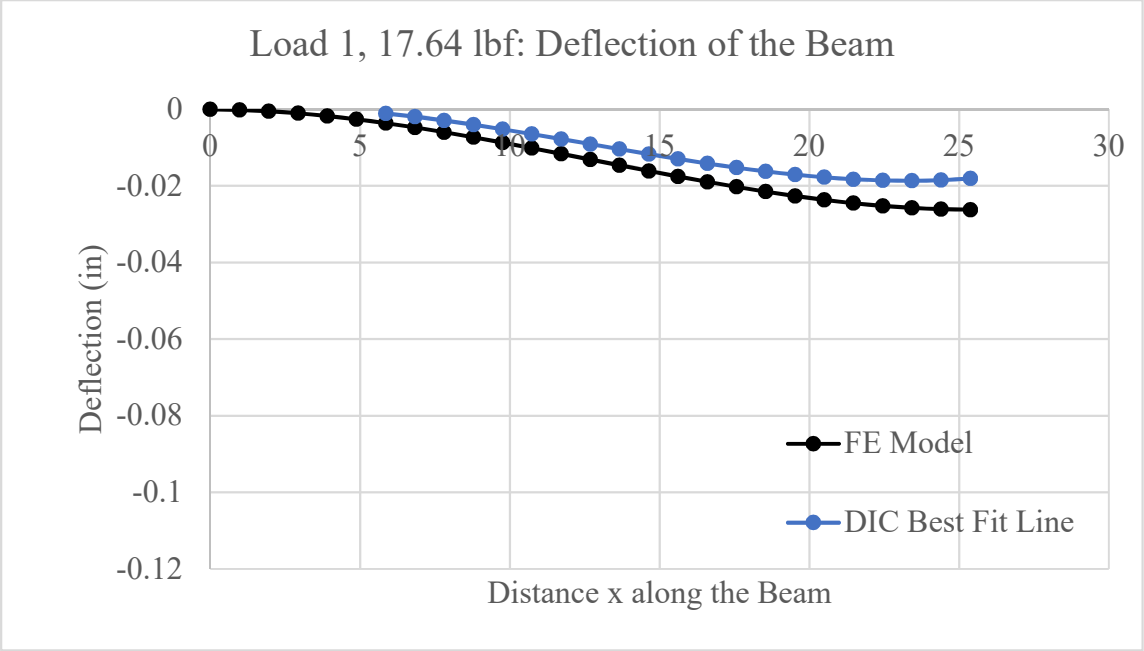

Figure 5.10. Load 1, 17.64 lbf: DIC Deflection Best Fit Line vs. FE Deflections

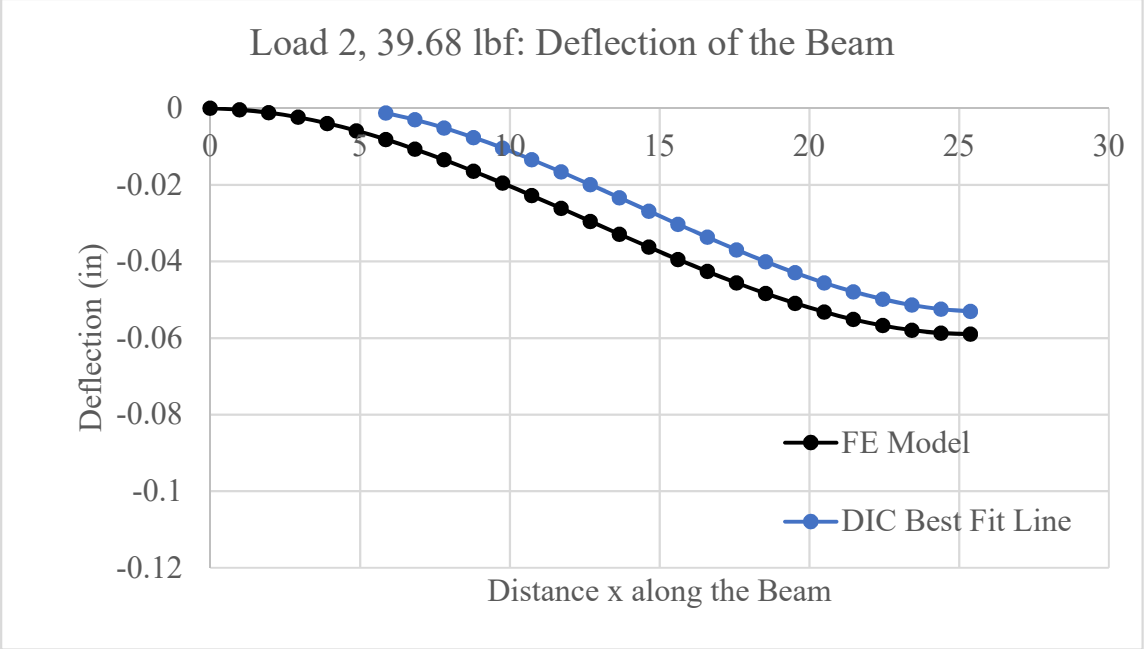

Figure 5.11. Load 2, 39.68 lbf: DIC Deflection Best Fit Line vs. FE Deflections

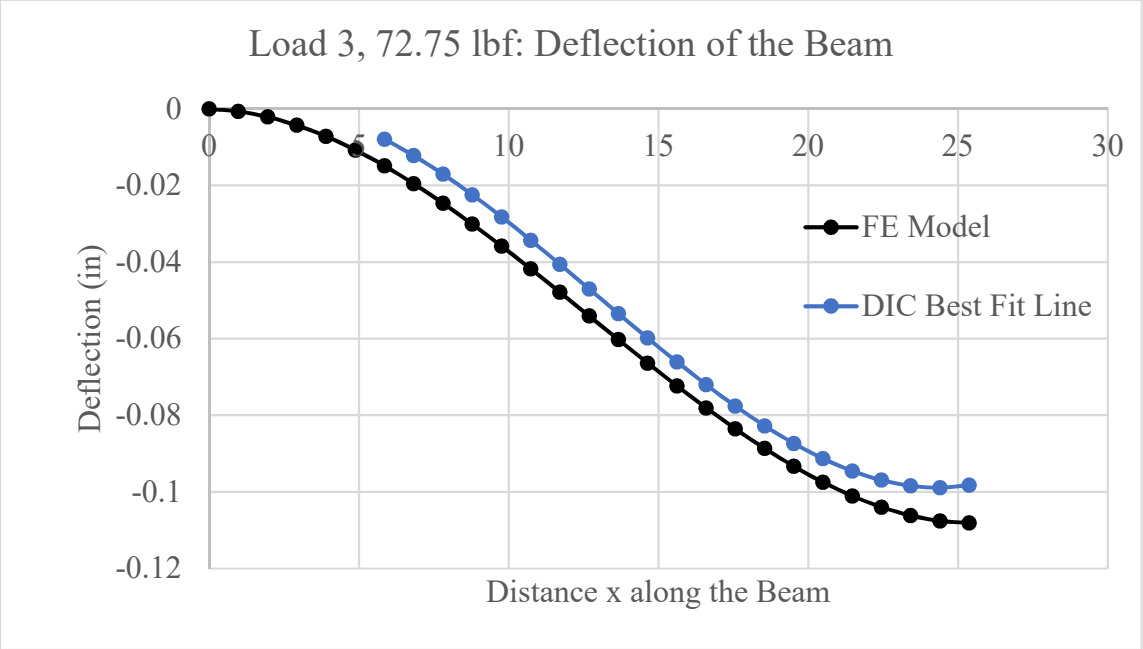

Figure 5.12. Load 3, 72.75 lbf: DIC Deflection Best Fit Line vs. FE Deflections

In addition, the absolute differences between the DIC and FE deflection were calculated for all three loads along the distance of the beam in Table 5.1. Furthermore, absolute percent errors were calculated for all three loads along the distance of the beam and plotted in Figure 5.13.

Table 5.1. Absolute Difference between FE and DIC Deflections

	Absolute Difference between DIC and FE Deflections (in)		
Distance x (in)	*Load 1, 17.64 lbf*	*Load 2, 39.68 lbf*	*Load 3, 72.75 lbf*
5.856	0.002538	0.005152	0.006996
6.832	0.002812	0.005540	0.007365
7.808	0.003057	0.005828	0.007577
8.784	0.003280	0.006025	0.007654
9.760	0.003484	0.006144	0.007618
10.736	0.003675	0.006195	0.007492
11.712	0.003857	0.006188	0.007298
12.688	0.004036	0.006133	0.007058
13.663	0.004215	0.006042	0.006793
14.639	0.004399	0.005925	0.006528
15.615	0.004594	0.005794	0.006284
16.591	0.004804	0.005658	0.006083
17.567	0.005033	0.005528	0.005948
18.543	0.005286	0.005414	0.005900
19.519	0.005569	0.005328	0.005964
20.495	0.005885	0.005280	0.006159
21.471	0.006240	0.005281	0.006506
22.447	0.006639	0.005342	0.007035
23.423	0.007085	0.005470	0.007758
24.399	0.007581	0.005674	0.008700
25.375	0.008128	0.005954	0.009854

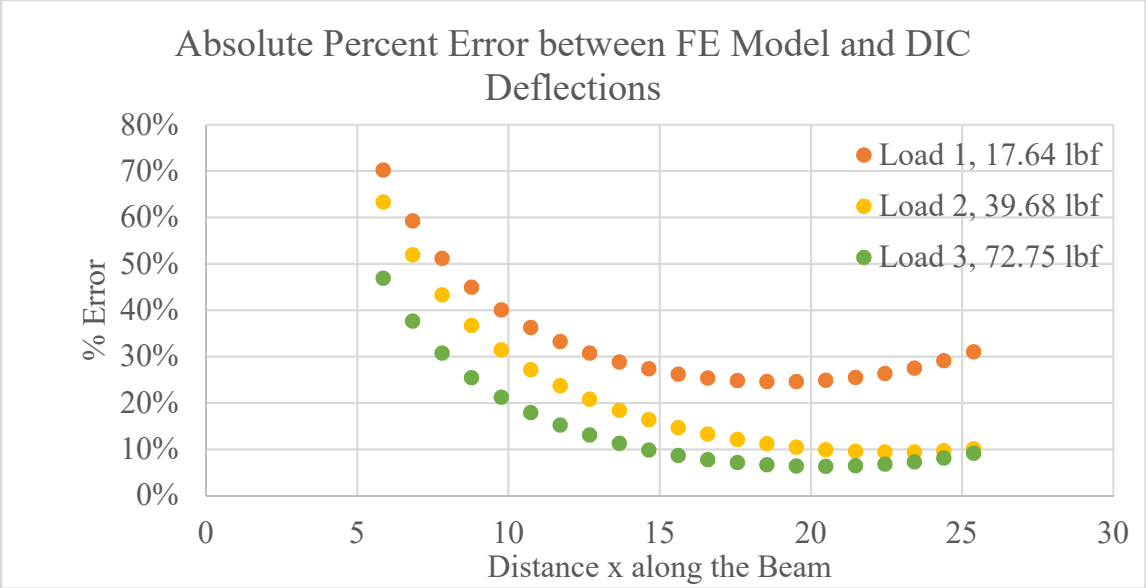

Figure 5.13. All Loads: Absolute Percent Error between FE and DIC Deflections

For load 1, as the distance along the beam was increased, the calculated difference between the FE model and DIC deflections increased. Furthermore, for load 2, absolute percent errors decreased as the distance along the beam increased. Moreover, for load 3, the absolute percent error decreased until a minimum error at 20 inches was encountered. After this 20 inch distance along the beam was reached then a subsequent increase in percent error was seen. In addition, it was apparent that as the load applied was increased, there was a general decrease in absolute percent errors between DIC and FE deflections. The average difference between DIC and FE model deflections were 0.004866, 0.005709, and 0.007075 inches. for loads 1, 2, and 3 respectively. The absolute average percent error DIC and FE model deflections were 34%, 22%, and 15%. for loads 1, 2, and 3 respectively.

Based on this analysis, the largest discrepancy between the two data sets was towards midspan for loads 2 and 3 and near the quarter point for load 1.

Differences between all three data sets were investigated. Differences occurred as a result of both DIC and FE model errors. The columns, brackets, and gusset plates were not modeled in the FE software which resulted in an assumption of a continuous moment of inertia and stiffness throughout the entire model. Furthermore, by not modeling the entire frame system, rotation in the columns were not modeled. In modeling the entire frame, a better analysis and representation of the structure could have been performed. By modeling all elements of the frame, greater FE model deflections would have been achieved. Therefore, this improvement would have resulted in less differences between FE and analytical solutions as well as FE and DIC differences. In addition, the self-weight of the beam was not implemented within the FE model. By implementing the self-weight of the beam, higher deflection would have been experienced, reducing the differences in deflections when compared. DIC errors are discussed in section 5.3 of this paper.

5.2. Comparisons of Strain Results

For both DIC FOVs, strain data was extracted for comparison for all three load cases. The two FOV's were combined as done previously to represent the beams midspan in its entirety. Figure 5.14, Figure 5.15, and Figure 5.16 represent the raw DIC deflection data from loads 1, 2, and 3 respectively.

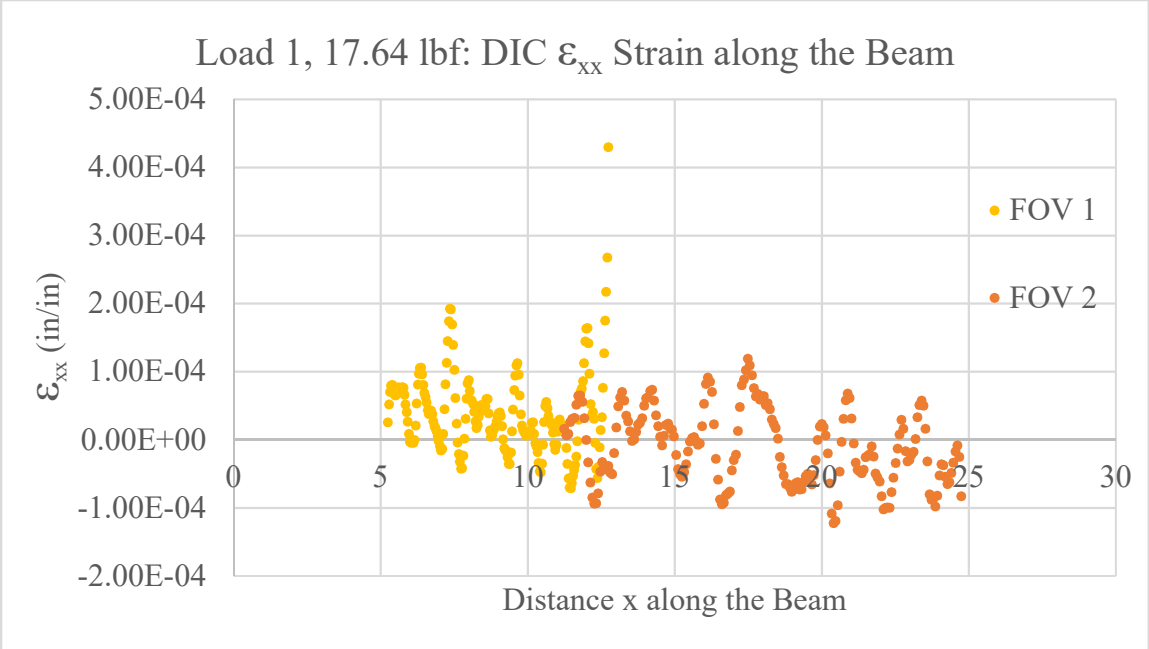

Figure 5.14. Load 1, 17.64 lbf: FOV 1 & 2 DIC Strains

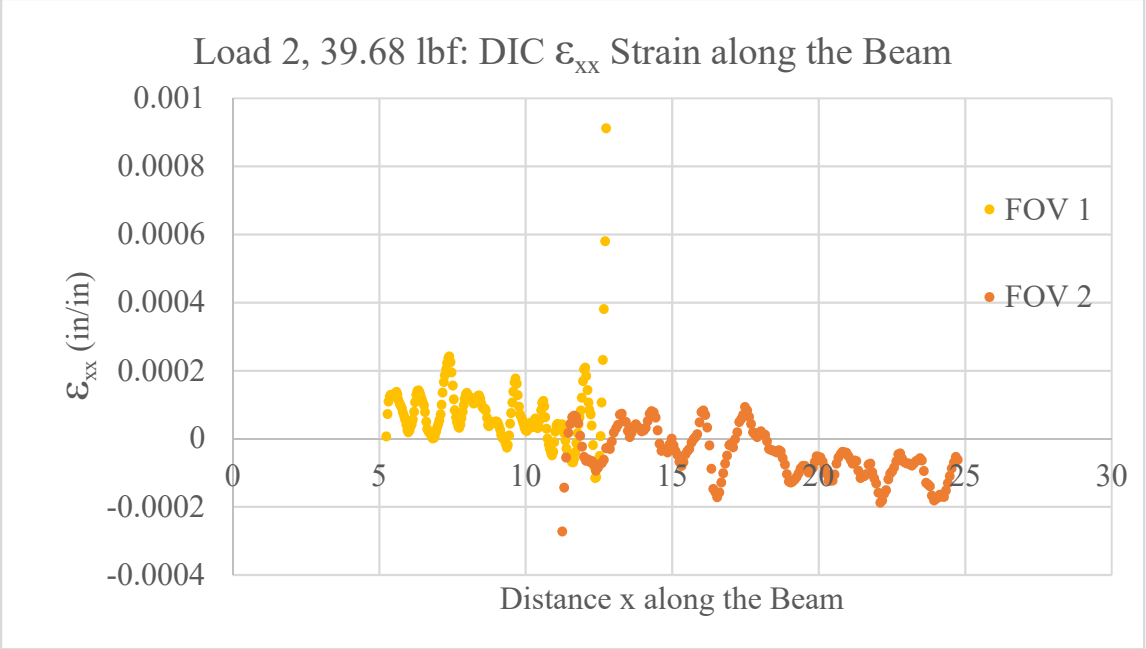

Figure 5.15. Load 2, 39.68 lbf: FOV 1 & 2 DIC Strains

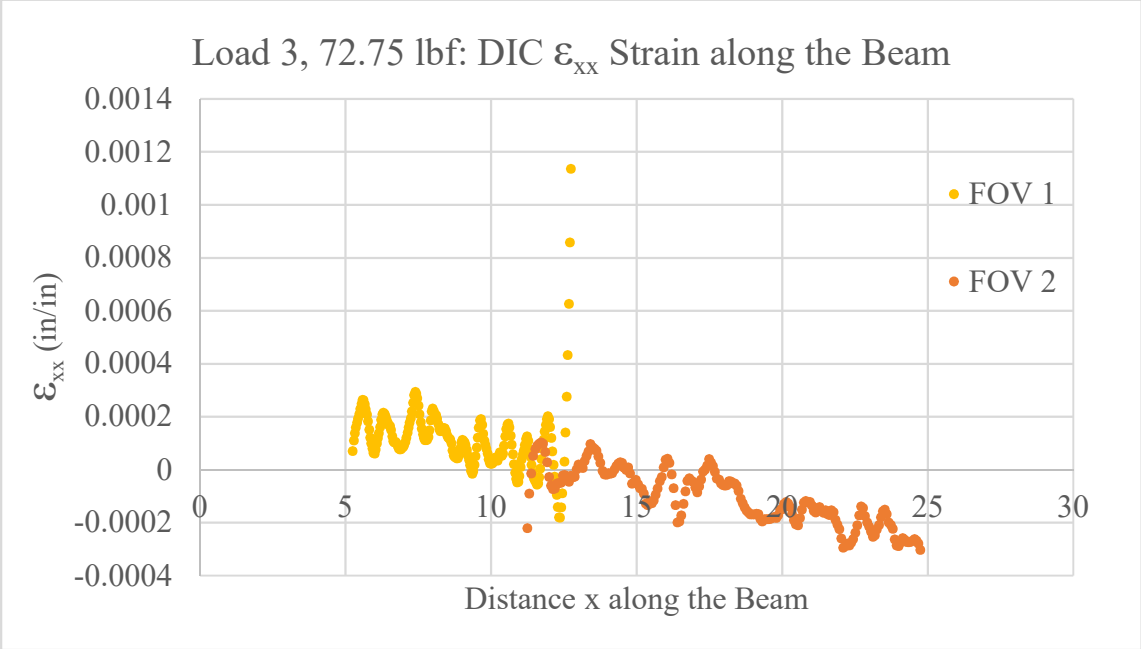

Figure 5.16. Load 3, 72.75 lbf: FOV 1 & 2 DIC Strains

For Load 1, as depicted in Figure 5.14, the strain values ranged from approximately -0.00001 to 0.00004. In addition, for Load 2, shown in Figure 5.15, the strain values ranged approximately from -0.0003 to 0.001. Lastly, Load 3 strain values ranged approximately from -0.0003 to 0.0012. It was apparent that there were inconsistencies in the DIC strain values for all loads. Therefore, when comparing to the FE model, there was a great amount of error and discrepancy between the two data sets. As a result, the comparison using the strain values between DIC and FE was unsuccessful.

Although the comparison between the strain values was unsuccessful, a comparison between the deflection values of the beams proved to be successful with low calculated

differences. Therefore, strain equations were derived by using Euler Bernoulli Theory. The Euler Bernoulli relationship stated the strain in a beam at a point is the second derivative of the deflection multiplied by the distance to the neutral axis. Many assumptions were made including that the deflections were minimal, and that the beam's cross section remains normal and planar to the deformed axis. Understanding the relationship between deflection and strain in the beam, the second derivative of the deflection best fit line was taken to determine the strain equation for each load case in the AOI per Equation (4-9).

$$\varepsilon(x)_1 = -1 * (0.000024x - 0.000304) \quad \text{Equation (5-1)}$$

$$\varepsilon(x)_2 = -1 * (0.000054\text{x} - 0.000724) \quad \text{Equation (5-2)}$$

$$\varepsilon(x)_3 = -1 * (0.000102\text{x} - 0.00132) \quad \text{Equation (5-3)}$$

Equations (5-1-), (5-2), and (5-3) represent derived strain along the beam for loads 1, 2, and 3 respectively. These equations were second degree polynomials which were then plotted with the FE model to investigate the relationship between strain data sets. Figures 5.17, 5.18, and 5.19 present successful relationships between DIC and FE model strains.

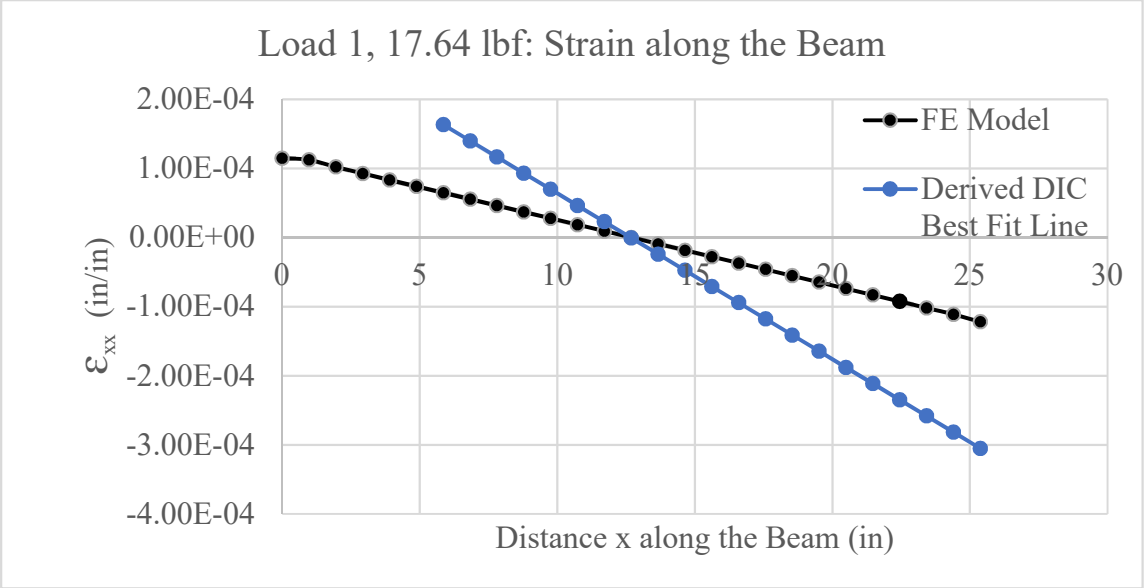

Figure 5.17. Load 1, 17.64 lbf: FE vs. Derived DIC Strains

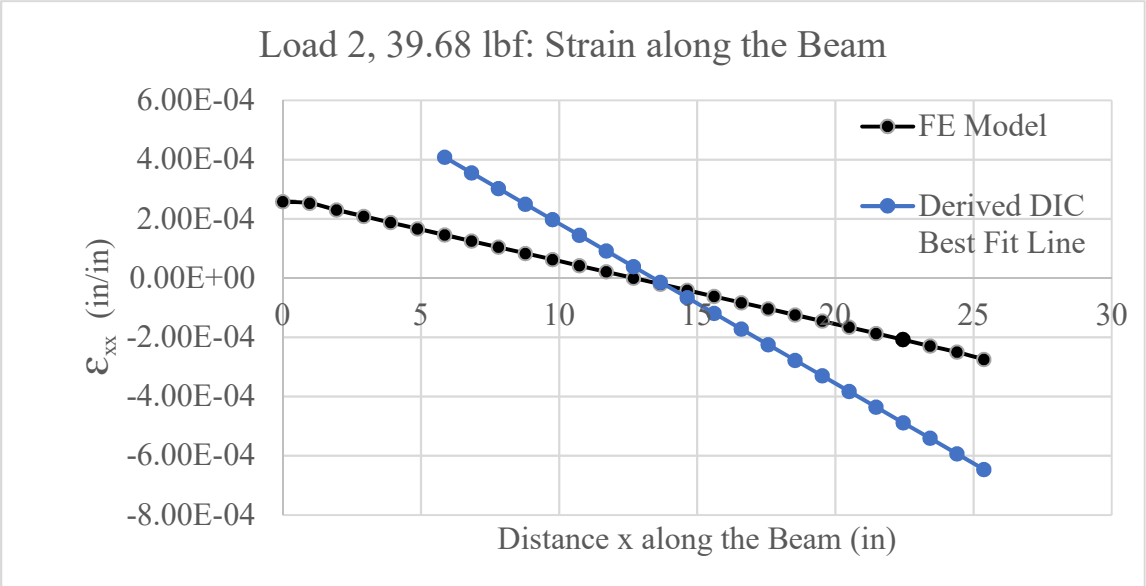

Figure 5.18. Load 2, 39.68 lbf: FE vs. Derived DIC Strains

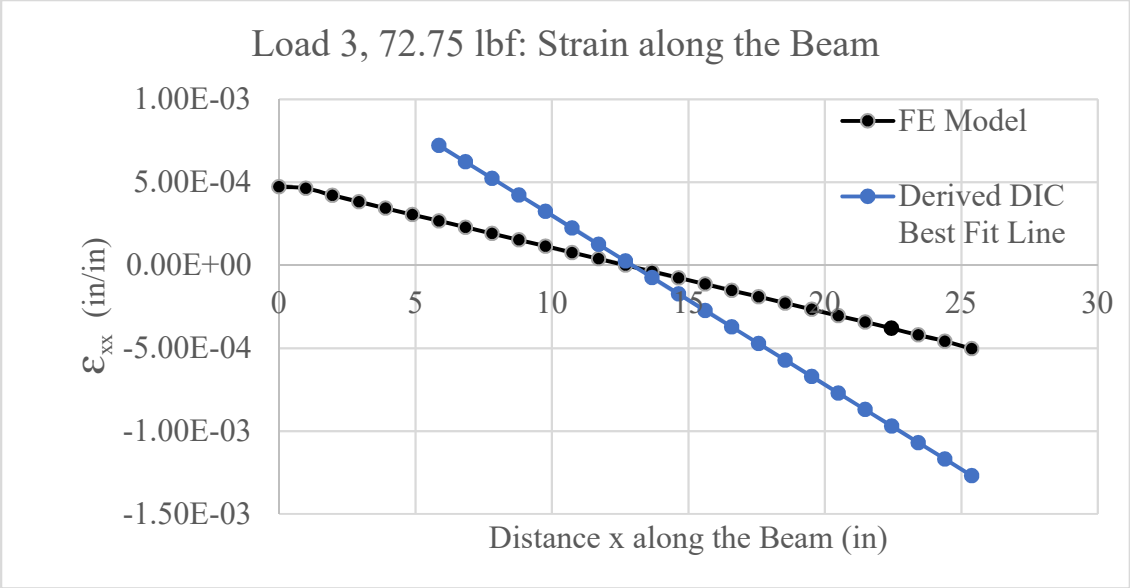

Figure 5.19. Load 3, 72.75 lbf: FE vs. Derived DIC Strains

By using the relationship between deflection and strain, strain curves were developed for analysis. For load 1, the average absolute difference between the two curves was 0.000080 strain.. The minimum and maximum absolute differences of strain for load 1 were 0.000001 and 0.000183. Moreover, the average, minimum, and maximum absolute strain differences for load 2 were 0.00017249, 0.000007, and 0.000372 respectively. Lastly for load 3, the average, minimum, and maximum absolute differences of strain were 0.000342, 0.0000025, and 0.000765. The absolute average percent errors between the FE and derived DIC strains for loads 1, 2, and 3 were 63%, 58%, 63% respectively. The highest points of difference occurred at the fixed end and the midspan of the beam for all three loads. The maximum difference occurred midspan of the beam across all loads. Furthermore, the minimum difference occurred at the points of intersection between the

FE and DIC strains. This intersection occurred near the quarter point of the beam, at the inflection point, for all three loads. The inflection point of the beam is defined as a point where the moment experienced by the beam is zero. Since the moment is zero, the stress in the beam is zero and therefore the strain at that point is zero.

Error in the derived strain equations may be as a result of estimation when performing the derivation of the deflection. Since strain was at a much smaller scale than the deflection, by deriving this function, the error experienced was larger when compared to a smaller value of strain. Also, with every derivation of the deflection equation, the higher the error due to estimation. Furthermore, the assumptions regarding Euler Bernoulli's equation may not be accurate and the beam may have deformed and rotated along the axis z-axis.

5.3. Sources of Error in DIC Data

The noise experienced in the data may be a result of the following:

- Vibrations experienced during the loading/photographing of the beam
- DIC's inability to capture small strain values
- DIC's inability to capture the complicated geometry of the section
- High light reflectivity on the surface of the photographed area
- Construction errors resulting in the movement of the beam
- Inadequate speckle pattern

The back and forth movement of the beam during loading may have resulted in alternating direction of strains causing the oscillating behavior in the data. In addition, the strain magnitudes on the beam may have been too small to be captured accurately.

According to the manufacturer of the DIC equipment, a strain precision for DIC is 100 micro-strain. However, depending on the speckle pattern accuracy, equipment setup, lighting, and image quality, this precision may be reduced. Furthermore, due to the complex cross-sectional geometry of the beam, the system had difficulty tracking speckle deformation. Moreover, due to the darkness of the room the experiment was performed in, spotlights were required to illuminate the surface of the specimen. This light caused high reflectively on the surface which resulted in noisy data.

It was believed that the highest source of error occurred as a result of the speckle pattern. Due to the small area of interest but a large FOV, the selection of the speckle pattern may have been insufficient. Using a smaller speckle pattern dot size and a smaller FOV may have resulted in higher accuracy. In addition, application of the speckle pattern may not have been adequate for fine-scale strain measurements. Upon further evaluation of the speckle pattern, areas of speckle bias were noted. In addition, there were a few areas of speckle that were merged which may have caused false matching. These areas are displayed in Figure 5.20.

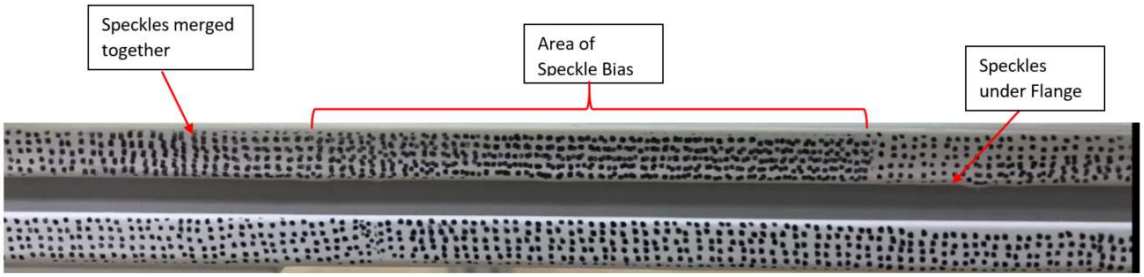

Figure 5.20. Error Due to Speckle Pattern

Lastly, construction error may have resulted in inefficient DIC measurement. According to the DIC results, less deflection was experienced by the beam compared to the FE model under equal loading. Therefore, the assumption of the boundary conditions being fixed-fixed may have been inaccurate. It appears that the system exerted strain and upward deflection on the beam resulting from over-stiffening at the column to beam connection. This was caused by system fabrication error and led to differences between FE and DIC results which must be addressed in future work.

5.4. Preliminary Test of FE Model Updating

Further investigation into the optimization of boundary conditions and the constitutive properties of the system must be completed. While this work is out of the scope of this thesis, a preliminary test to determine viability was performed. DIC and FE model results varied notably near midspan. This was believed to have been caused by insufficient modeling of the beam to column connections. Therefore, the FE model was updated in ANSYS. The update included increasing the stiffness of the beam within 5.075 inches of the support. The 5.075 inch extent of this increase was based on the length of the L-stiffener. This update was to refine the FE model to show a larger stiffening at the column to beam connection due to the installation of L-brackets and gusset plates. Furthermore, since the gusset plates and bracket were made of steel, a higher modulus of elasticity was expected at the end points of the beam. This was accomplished by increasing the beam's

modulus of elasticity from 10,200,000 to 11,650,000 pounds per square inch, in this section. Figure 5.20 displays the updated material in green.

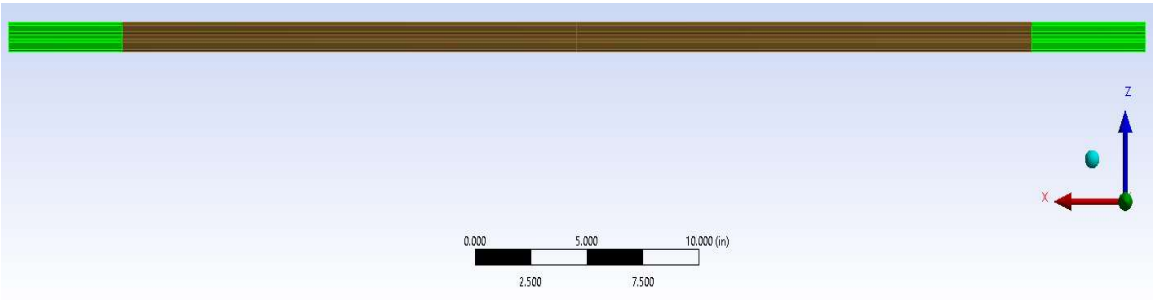

Figure 5.21. Updated FE Model

The increased modulus of elasticity value was determined by incrementally increasing the stiffness until the midspan deflection point matched within 1 % to that of DIC. As a result, absolute difference between the DIC deflection and the updated FE model was reduced overall. Table 5.2 shows this reduction in the absolute differences through this basic optimization.

Table 5.2. Reduction in Absolute Differences of Deflection

	Absolute Difference		
Distance x (in)	*DIC vs Initial FE Model*	*DIC vs Updated FE Model*	**Type of Change**
5.856	0.006996	0.002765	DECREASE
6.832	0.007365	0.002126	DECREASE
7.808	0.007577	0.001357	DECREASE

8.784	0.007654	0.000513	DECREASE
9.760	0.007618	0.000356	DECREASE
10.736	0.007492	0.001207	DECREASE
11.712	0.007298	0.002003	DECREASE
12.688	0.007058	0.002712	DECREASE
13.663	0.006793	0.003308	DECREASE
14.639	0.006528	0.003772	DECREASE
15.615	0.006284	0.004089	DECREASE
16.591	0.006083	0.004254	DECREASE
17.567	0.005948	0.004263	DECREASE
18.543	0.005900	0.004121	DECREASE
19.519	0.005964	0.003838	DECREASE
20.495	0.006159	0.003431	DECREASE
21.471	0.006506	0.002923	DECREASE
22.447	0.007035	0.002340	DECREASE
23.423	0.007758	0.001717	DECREASE
24.399	0.008700	0.001095	DECREASE
25.375	0.009854	0.000520	DECREASE

As shown in Table 5.2, improvement in the relationship between the DIC deflection and FE model was achieved. The average difference for the initial FE model comparison to DIC was 0.007075 inch. This average difference was reduced by 0.004565 inch resulting in a 0.002510 inch average difference when comparing DIC to the updated FE model. This proves that by performing basic optimization methods, an improved relationship is feasible overall. More sophisticated optimization methods must be investigated and require further research.

CHAPTER 6: CONCLUSIONS

The purpose of this thesis was to determine the feasibility of DIC as a FEMU tool. In order to test this, an experimental investigation on an aluminum frame was conducted. A series of tests were conducted on the frame by loading the frame incrementally at midspan. Images were captured by DIC for processing for two field of views encasing approximately half of the beam. In conjunction, an FE model of the structure was developed in ANSYS for which the same loads were applied. Analytical solutions of strain and deflection were derived using Hooke's law and the Euler Bernoulli beam theory. A comparison was then performed between DIC and analytical solutions, FE model and analytical solutions, and DIC and the FE model.

6.1. Conclusions

Comparisons between the FE model and DIC data were completed based on deflection and strain parameters. Initially, the FE model and DIC deflection data were checked against analytically derived solutions. Both systems compared highly to analytical solutions. For the FE model and analytical deflections, average absolute differences less than 0.002 inches were calculated. In addition, the absolute average percent error between the FE model and analytical deflections was approximately 6%. Furthermore, the average absolute differences between DIC and analytical solutions of deflection were less than 0.005 inches resulting in absolute average percent error less than 33%. With regards to DIC strain data, there was too much error for comparison. Therefore, by using the relationship

between strain and deflection, a best fit line for strain was extracted from deflection and resulted in a good relationship. Furthermore, a comparison between DIC and a FE model was performed.

The comparison between DIC and FE model deflections was feasible and led to average absolute differences between 0.004866 and 0.007075 inches and absolute average percent errors between 15% and 34%. For deflection and strain, the largest differences occurred towards midspan. It was also noted that the lowest point of error for strain occurred at approximately one-quarter length of the beam. At this point, both the DIC data and the model had an inflection point. Overall, DIC's ability to be used as a FEMU tool was accomplished however, further research is required into the limitations and optimization of the method.

6.2. Limitations

Throughout the experiment, sources of error between the FE model and DIC data were identified. The DIC strain data was too noisy for calibration and may have been a result of vibrations experienced during the loading of the beams, DIC's inability to capture such small strain values, DIC's inability to capture the complicated geometry of the section, high light reflectivity on the surface of the photographed area, construction errors resulting in the movement of the beam, and speckle pattern inadequacy. It is believed that the speckle pattern contributed highly to the noise in the data. Upon further inspection, areas of speckle bias and speckle overlapping were identified. Furthermore, assumptions regarding the boundary conditions of the beam proved to be inadequate. Due to overstraining and the complexity of the beam to column connections, strain and upward deflection were believed

to be exerted onto the beam ends. This led to error between the FE model and the DIC data. In addition, by only modeling the beam, the stiffness and moment of inertia at the fixed ends were not adequately captured. Furthermore, if the entire frame was modeled, greater deflection values would have occurred, reducing the differences between the FE and DIC results as well as the FE and analytical results of deflection and strain. In order to understand the extent and improve calibration techniques, each error must be further investigated in future work.

6.3. Recommendations for Future Work

Future research for this topic includes correlating the model to DIC by optimally changing boundary conditions and material properties of the FE model. It was clear through this experiment that the highest points of difference occurred at midspan. Therefore, investigation into the best approach for modeling the boundary conditions must be completed. Methods that may be investigated include using springs with stiffness values. In addition, by adjusting the geometric or material properties of the structure, successful relationship may be achieved. By increasing the moment of inertia of the beam, stiffer boundary conditions can be achieved that are more representative of the structure. This can also be achieved by changing the modulus of elasticity near the beam ends. An initial basic optimization was performed to determine feasibility of this approach. The modulus of elasticity at the ends of the beam was increased to represent stiffer connections. In doing so, absolute differences in deflection between DIC and FE model deflections was reduced overall with the average difference decreasing by 0.004565 inches. Another factor that must be investigated is an attempt to model the gusset plates, L-stiffeners, and columns

within the FE model. In doing so, a better representation of the structure would be achieved. Furthermore, a test for the entire frame should be investigated. By testing the entire frame better deflection and strain results can be compared. Further research must be done to determine different methods of optimization. Future work in this area may lead to improved methods of using DIC for structural health monitoring.

APPENDIX A: DIC FOV 1 DATA

Table A.1. Load 1: Raw DIC Deflection and Strain Data for FOV 1

Distance x along the Beam (inches)	Average Deflection (inches)	Average ε_{xx} Strain (in/in)
5.25	-0.000967085	2.53836E-05
5.287688442	-0.000993441	5.15706E-05
5.325376884	-0.001024704	6.99184E-05
5.363065327	-0.001062228	0.000079548
5.400753769	-0.001083913	8.03112E-05
5.438442211	-0.001094557	7.48826E-05
5.476130653	-0.001111057	6.64444E-05
5.513819095	-0.001133198	0.000064944
5.551507538	-0.001151102	6.99334E-05
5.58919598	-0.001179474	0.000076736
5.626884422	-0.001224197	7.66764E-05
5.664572864	-0.001261251	0.0000712
5.702261307	-0.001284906	0.00007184
5.739949749	-0.001304691	0.00007712
5.777638191	-0.001327627	0.0000763
5.815326633	-0.001348794	0.00006574
5.853015075	-0.001366124	0.00005192
5.890703518	-0.001384935	0.00004024
5.92839196	-0.001406332	0.000026102
5.966080402	-0.001437687	0.00000867
6.003768844	-0.001470965	-0.00000308
6.041457286	-0.00148913	-0.00000458
6.079145729	-0.001504872	-0.0000034
6.116834171	-0.001543131	-0.00000488
6.154522613	-0.001583635	-6.6E-07
6.192211055	-0.001611303	0.000020492
6.229899497	-0.001630062	0.00005324

6.26758794	-0.001648702	8.08456E-05
6.305276382	-0.001671549	0.000096867
6.342964824	-0.001690591	0.000105121
6.380653266	-0.001711704	0.000105648
6.418341709	-0.001749476	9.60324E-05
6.456030151	-0.001803476	8.04442E-05
6.493718593	-0.001861631	6.86264E-05
6.531407035	-0.00190355	6.25754E-05
6.569095477	-0.001919061	5.42752E-05
6.60678392	-0.001923429	0.00004304
6.644472362	-0.001935789	0.0000376
6.682160804	-0.00196562	0.00004038
6.719849246	-0.002011372	4.28298E-05
6.757537688	-0.002062826	0.000037398
6.795226131	-0.002104866	2.68842E-05
6.832914573	-0.002129434	1.96826E-05
6.870603015	-0.002142392	1.71004E-05
6.908291457	-0.00216086	1.25418E-05
6.945979899	-0.002198018	5.0934E-06
6.983668342	-0.002243232	-2.4522E-06
7.021356784	-0.002275664	-9.6786E-06
7.059045226	-0.002297794	-0.0000162
7.096733668	-0.002311083	-0.000013456
7.134422111	-0.002335309	0.000008522
7.172110553	-0.0023791	0.00004454
7.209798995	-0.00242132	8.12104E-05
7.247487437	-0.002454191	0.000112963
7.285175879	-0.002488136	0.000144923
7.322864322	-0.002547919	0.000174061
7.360552764	-0.002596485	0.000192146
7.398241206	-0.002636416	0.000191122
7.435929648	-0.002671804	0.000169286
7.47361809	-0.002720947	0.000139153
7.511306533	-0.002771961	0.000102546
7.548994975	-0.002796611	6.12848E-05
7.586683417	-0.002816954	0.000023647
7.624371859	-0.002830043	-0.00000442

7.662060302	-0.002868779	-2.12104E-05
7.699748744	-0.002919873	-0.000032346
7.737437186	-0.002960975	-0.000042612
7.775125628	-0.002986431	-4.16048E-05
7.81281407	-0.002992902	-0.000023642
7.850502513	-0.003003798	0.000001385
7.888190955	-0.003033633	0.000030756
7.925879397	-0.003097137	0.00006034
7.963567839	-0.003183246	8.26142E-05
8.001256281	-0.003240371	8.72488E-05
8.038944724	-0.003266176	7.13132E-05
8.076633166	-0.003291253	5.82098E-05
8.114321608	-0.003310696	5.61942E-05
8.15201005	-0.003341724	5.21598E-05
8.189698492	-0.003380235	0.000040944
8.227386935	-0.003440394	0.000026582
8.265075377	-0.003486786	0.000017079
8.302763819	-0.003513538	0.000021448
8.340452261	-0.003537146	3.38916E-05
8.378140704	-0.003592404	4.46464E-05
8.415829146	-0.003655934	5.06416E-05
8.453517588	-0.003705232	4.98652E-05
8.49120603	-0.003748391	4.49236E-05
8.528894472	-0.00378788	0.000043082
8.566582915	-0.003823535	4.89774E-05
8.604271357	-0.003855435	0.000059897
8.641959799	-0.00388928	5.96982E-05
8.679648241	-0.003933189	0.00003832
8.717336683	-0.003979016	0.0000138
8.755025126	-0.004022016	0.000004066
8.792713568	-0.004066622	0.00000651
8.83040201	-0.004112441	0.000012826
8.868090452	-0.00415189	0.00001666
8.905778894	-0.004187874	0.000019861
8.943467337	-0.004224126	2.66896E-05
8.981155779	-0.004253567	0.000033936
9.018844221	-0.004289709	3.87038E-05

9.056532663	-0.004340496	4.00684E-05
9.094221106	-0.004391244	0.00003462
9.131909548	-0.00443185	0.000019658
9.16959799	-0.004457504	0.000000494
9.207286432	-0.004490709	-0.000012608
9.244974874	-0.004533252	-0.00001536
9.282663317	-0.004570717	-0.000016718
9.320351759	-0.004611213	-0.00002582
9.358040201	-0.004656606	-0.00003578
9.395728643	-0.004702677	-0.00003592
9.433417085	-0.004749173	-0.000018744
9.471105528	-0.004791819	0.00001204
9.50879397	-0.004839047	0.00004424
9.546482412	-0.004880638	0.000072894
9.584170854	-0.004916276	9.42076E-05
9.621859296	-0.004959559	0.000108911
9.659547739	-0.00501174	0.000112435
9.697236181	-0.005060906	0.000095374
9.734924623	-0.005106197	6.49076E-05
9.772613065	-0.005151173	3.72882E-05
9.810301508	-0.005197827	0.000020513
9.84798995	-0.005236504	1.42348E-05
9.885678392	-0.005271606	1.15018E-05
9.923366834	-0.005306717	8.04E-06
9.961055276	-0.005341071	5.6144E-06
9.998743719	-0.005371843	7.1618E-06
10.03643216	-0.005425811	8.1542E-06
10.0741206	-0.005489	0.0000081
10.11180905	-0.005545598	0.000013284
10.14949749	-0.005587803	0.000024754
10.18718593	-0.005639787	2.53754E-05
10.22487437	-0.005697654	0.00000822
10.26256281	-0.005752291	-0.0000053
10.30025126	-0.005789984	-0.000009178
10.3379397	-0.005813921	-0.0000182
10.37562814	-0.005846307	-3.41608E-05
10.41331658	-0.005899803	-4.65036E-05

10.45100503	-0.005942008	-4.79818E-05
10.48869347	-0.005971244	-3.52426E-05
10.52638191	-0.006006866	-0.000007334
10.56407035	-0.006077433	2.59216E-05
10.60175879	-0.00614652	4.93804E-05
10.63944724	-0.006189724	5.52458E-05
10.67713568	-0.006221228	0.000046079
10.71482412	-0.006246142	0.00003484
10.75251256	-0.006275157	0.0000269
10.79020101	-0.006324724	0.00002396
10.82788945	-0.006396362	0.00002132
10.86557789	-0.006465732	0.00001024
10.90326633	-0.006507843	-0.0000065
10.94095477	-0.006537882	-0.000015216
10.97864322	-0.006577236	-0.000007718
11.01633166	-0.006623433	0.00001157
11.0540201	-0.006659181	0.00002736
11.09170854	-0.006695386	0.000029448
11.12939698	-0.006743126	0.000021994
11.16708543	-0.00679611	1.63888E-05
11.20477387	-0.006854654	0.000018824
11.24246231	-0.006920709	0.00002051
11.28015075	-0.006987598	0.000009164
11.3178392	-0.007041205	-0.000012392
11.35552764	-0.007075118	-0.00003576
11.39321608	-0.007105441	-0.000056872
11.43090452	-0.007150228	-0.000070296
11.46859296	-0.007209969	-7.12168E-05
11.50628141	-0.007275937	-6.33044E-05
11.54396985	-0.007332654	-5.32754E-05
11.58165829	-0.007372984	-4.47342E-05
11.61934673	-0.007402134	-3.71838E-05
11.65703518	-0.00743278	-2.48822E-05
11.69472362	-0.007473827	-0.00000218
11.73241206	-0.007511425	0.00002918
11.7701005	-0.007554921	5.75154E-05
11.80778894	-0.007619409	7.08918E-05

11.84547739	-0.007684827	7.49862E-05
11.88316583	-0.007737354	8.57762E-05
11.92085427	-0.007778575	0.000112092
11.95854271	-0.007829654	0.0001444
11.99623116	-0.007893047	0.000163167
12.0339196	-0.007962079	0.0001639
12.07160804	-0.008030543	0.000141599
12.10929648	-0.008079598	0.000096793
12.14698492	-0.008120622	0.00005216
12.18467337	-0.008163559	0.00003536
12.22236181	-0.008228094	0.00004058
12.26005025	-0.008284441	0.00003076
12.29773869	-0.008321213	-0.000004894
12.33542714	-0.008360378	-0.000043131
12.37311558	-0.008386787	-0.000056421
12.41080402	-0.008424213	-4.01524E-05
12.44849246	-0.008477071	-1.15088E-05
12.4861809	-0.008542827	0.000014038
12.52386935	-0.008606142	3.28524E-05
12.56155779	-0.008655921	0.000076341
12.59924623	-0.008702827	0.000126658
12.63693467	-0.008751528	0.000174672
12.67462312	-0.008814732	0.000217164
12.71231156	-0.008874543	0.000267305
12.75	-0.008929283	0.000429287

Table A.2. Load 2: Raw DIC Deflection and Strain Data for FOV 1

Distance x along the Beam (inches)	Average Deflection (inches)	Average ε_{xx} Strain (in/in)
5.25	-0.002655553	0.000006782
5.287688442	-0.002699306	0.000072944
5.325376884	-0.002755924	0.000109211
5.363065327	-0.002842926	0.000124733
5.400753769	-0.002901878	0.000129516
5.438442211	-0.002941243	0.000129358

5.476130653	-0.002991117	0.000126048
5.513819095	-0.003056548	0.00012816
5.551507538	-0.003115856	0.000134131
5.58919598	-0.003182222	0.000137652
5.626884422	-0.003262999	0.000129983
5.664572864	-0.003343824	0.000114551
5.702261307	-0.003409098	0.000103615
5.739949749	-0.003460229	9.72232E-05
5.777638191	-0.003515747	8.93318E-05
5.815326633	-0.003583827	7.78538E-05
5.853015075	-0.003654421	0.0000659
5.890703518	-0.003716261	0.00005542
5.92839196	-0.003766494	0.00004106
5.966080402	-0.003821429	0.000025486
6.003768844	-0.00387932	0.000019288
6.041457286	-0.00393522	0.000025098
6.079145729	-0.004002992	0.00003484
6.116834171	-0.004084874	0.0000437
6.154522613	-0.004166528	0.00005676
6.192211055	-0.004233362	0.00007948
6.229899497	-0.004286008	0.000107304
6.26758794	-0.004340693	0.000129117
6.305276382	-0.004413024	0.000140421
6.342964824	-0.00449863	0.000142206
6.380653266	-0.00458352	0.000136993
6.418341709	-0.004660236	0.00012798
6.456030151	-0.004734228	0.000116909
6.493718593	-0.004814976	0.000107498
6.531407035	-0.004894307	9.79696E-05
6.569095477	-0.00495637	0.00007824
6.60678392	-0.005006693	0.00005
6.644472362	-0.005063638	0.00002862
6.682160804	-0.005137252	0.00002096
6.719849246	-0.005223126	0.00001832
6.757537688	-0.005303362	0.00001264
6.795226131	-0.005381874	0.000005286
6.832914573	-0.00545337	0.000001106

6.870603015	-0.005518236	0.00000268
6.908291457	-0.005588654	0.000010022
6.945979899	-0.005670646	0.000021784
6.983668342	-0.005751354	0.000033468
7.021356784	-0.005814039	4.38448E-05
7.059045226	-0.005875504	5.50106E-05
7.096733668	-0.005944724	7.22862E-05
7.134422111	-0.006021843	0.000100487
7.172110553	-0.006109598	0.000135667
7.209798995	-0.006199165	0.000166819
7.247487437	-0.006276591	0.000186892
7.285175879	-0.006357756	0.000204052
7.322864322	-0.006457819	0.000222021
7.360552764	-0.006551803	0.000237284
7.398241206	-0.006633512	0.000241708
7.435929648	-0.00671348	0.000225205
7.47361809	-0.006821866	0.000194748
7.511306533	-0.006933039	0.00015637
7.548994975	-0.007020197	0.000115827
7.586683417	-0.007094181	8.39376E-05
7.624371859	-0.007157614	6.38102E-05
7.662060302	-0.007248992	0.00004896
7.699748744	-0.00735489	0.00003656
7.737437186	-0.007440063	0.000032178
7.775125628	-0.007507732	0.00004146
7.81281407	-0.007563921	6.03016E-05
7.850502513	-0.007629953	7.90914E-05
7.888190955	-0.007714591	9.88054E-05
7.925879397	-0.007831646	0.000117941
7.963567839	-0.007964299	0.000130871
8.001256281	-0.00807737	0.000135208
8.038944724	-0.008173157	0.000127074
8.076633166	-0.008262772	0.000120723
8.114321608	-0.008326031	0.000121362
8.15201005	-0.008389843	0.000117572
8.189698492	-0.008472606	0.000109492
8.227386935	-0.008588488	0.000104087

8.265075377	-0.008691882	0.0001056
8.302763819	-0.008782268	0.000112604
8.340452261	-0.008872315	0.000120095
8.378140704	-0.008991087	0.000126191
8.415829146	-0.009106268	0.000126913
8.453517588	-0.009203709	0.000117939
8.49120603	-0.009303441	0.000103754
8.528894472	-0.009399472	0.000092961
8.566582915	-0.009487205	8.87896E-05
8.604271357	-0.009570157	8.91324E-05
8.641959799	-0.009665008	8.26924E-05
8.679648241	-0.009775591	6.12394E-05
8.717336683	-0.009877449	0.00004112
8.755025126	-0.009966866	0.00003752
8.792713568	-0.010059173	0.0000441
8.83040201	-0.010158638	0.00004958
8.868090452	-0.010255339	0.00004866
8.905778894	-0.010349693	0.000046728
8.943467337	-0.010444102	0.00004902
8.981155779	-0.010528819	0.00005138
9.018844221	-0.010616181	0.000050242
9.056532663	-0.010718874	0.0000458
9.094221106	-0.010825315	0.00003838
9.131909548	-0.010916126	0.000026312
9.16959799	-0.010992543	0.00001182
9.207286432	-0.011089661	0.00000232
9.244974874	-0.011197047	2.6E-07
9.282663317	-0.01128926	-0.000002672
9.320351759	-0.011379528	-0.000014688
9.358040201	-0.011480787	-0.00002548
9.395728643	-0.01158622	-1.86052E-05
9.433417085	-0.011689921	0.00000962
9.471105528	-0.011787937	4.48988E-05
9.50879397	-0.011882606	7.53434E-05
9.546482412	-0.011977055	0.000106678
9.584170854	-0.012070126	0.000138778
9.621859296	-0.012169354	0.000166067

9.659547739	-0.012282748	0.000177565
9.697236181	-0.012404929	0.000162013
9.734924623	-0.012527	0.000127998
9.772613065	-0.012630315	9.41158E-05
9.810301508	-0.012722969	7.22462E-05
9.84798995	-0.012818819	6.34054E-05
9.885678392	-0.01291789	0.000057118
9.923366834	-0.013023276	4.60984E-05
9.961055276	-0.013120953	3.34456E-05
9.998743719	-0.013223858	0.00002542
10.03643216	-0.013348969	2.28132E-05
10.0741206	-0.013484394	0.000027522
10.11180905	-0.013601181	0.000037025
10.14949749	-0.013687063	4.67484E-05
10.18718593	-0.013778457	0.000045262
10.22487437	-0.01388174	3.46478E-05
10.26256281	-0.013999102	3.68152E-05
10.30025126	-0.014107528	5.45138E-05
10.3379397	-0.014201591	6.00422E-05
10.37562814	-0.014298693	4.55248E-05
10.41331658	-0.014422543	3.12384E-05
10.45100503	-0.014535457	3.47114E-05
10.48869347	-0.014627803	0.000056159
10.52638191	-0.014730969	8.43568E-05
10.56407035	-0.014871417	0.000105849
10.60175879	-0.015014323	0.000111083
10.63944724	-0.015126929	0.000095681
10.67713568	-0.015211236	6.37432E-05
10.71482412	-0.015298079	2.93496E-05
10.75251256	-0.015392669	6.7E-07
10.79020101	-0.015516173	-0.000017765
10.82788945	-0.015655441	-0.00002937
10.86557789	-0.015783165	-0.000041678
10.90326633	-0.015876142	-4.87338E-05
10.94095477	-0.015957315	-0.00003786
10.97864322	-0.016051079	-0.000009624
11.01633166	-0.016160244	0.000020961

11.0540201	-0.016270276	3.93194E-05
11.09170854	-0.016382205	4.31776E-05
11.12939698	-0.016498654	0.000039242
11.16708543	-0.016618622	0.000036274
11.20477387	-0.016738071	0.00003946
11.24246231	-0.016865165	4.23164E-05
11.28015075	-0.016992945	0.000034035
11.3178392	-0.017100803	0.000016154
11.35552764	-0.017185669	-0.00000528
11.39321608	-0.01726378	-0.000028254
11.43090452	-0.017359378	-4.71394E-05
11.46859296	-0.017481906	-5.49526E-05
11.50628141	-0.017618024	-0.000055652
11.54396985	-0.017742394	-0.000060064
11.58165829	-0.017846591	-0.000068067
11.61934673	-0.017944236	-0.00006916
11.65703518	-0.018044866	-0.000059116
11.69472362	-0.018146953	-0.0000394
11.73241206	-0.018240803	-0.00001268
11.7701005	-0.018342638	0.000016392
11.80778894	-0.018468811	4.25474E-05
11.84547739	-0.018593882	6.22172E-05
11.88316583	-0.018706323	8.29006E-05
11.92085427	-0.018822992	0.000120739
11.95854271	-0.01894978	0.000169953
11.99623116	-0.019080969	0.000204205
12.0339196	-0.019200583	0.000209226
12.07160804	-0.019328	0.000184374
12.10929648	-0.019449913	0.000143104
12.14698492	-0.019556992	0.000106716
12.18467337	-0.019664654	8.54326E-05
12.22236181	-0.019802551	7.14428E-05
12.26005025	-0.019932819	0.00003904
12.29773869	-0.020031866	-0.000018706
12.33542714	-0.02012448	-8.00572E-05
12.37311558	-0.02022437	-0.000115422
12.41080402	-0.020348953	-0.000112433

12.44849246	-0.020475449	-8.57022E-05
12.4861809	-0.020598094	-6.22328E-05
12.52386935	-0.020714039	-4.98924E-05
12.56155779	-0.020820386	8.0024E-06
12.59924623	-0.020923213	0.000106521
12.63693467	-0.021034685	0.000231367
12.67462312	-0.021166953	0.000381219
12.71231156	-0.021307646	0.000579905
12.75	-0.02142963	0.000911986

Table A.3. Load 3: Raw DIC Deflection and Strain Data for FOV 1

Distance x along the Beam (inches)	Average Deflection (inches)	Average Ɛxx Strain (in/in)
5.25	-0.006454606	6.96806E-05
5.287688442	-0.00658963	0.000109518
5.325376884	-0.006727551	0.000137774
5.363065327	-0.006876244	0.000159087
5.400753769	-0.007015685	0.000176573
5.438442211	-0.007138173	0.000193319
5.476130653	-0.007251709	0.000209351
5.513819095	-0.007369772	0.000228889
5.551507538	-0.007495583	0.000248946
5.58919598	-0.007642882	0.000263391
5.626884422	-0.007813748	0.000261981
5.664572864	-0.007978614	0.000245426
5.702261307	-0.008115984	0.000226576
5.739949749	-0.00824063	0.000206954
5.777638191	-0.008384228	0.000181904
5.815326633	-0.008536551	0.000150015
5.853015075	-0.008682236	0.0001197
5.890703518	-0.008830331	9.84248E-05
5.92839196	-0.008973039	7.92868E-05
5.966080402	-0.009112606	0.00006198

6.003768844	-0.009245134	0.00005952
6.041457286	-0.009378535	7.57988E-05
6.079145729	-0.009527543	9.84774E-05
6.116834171	-0.009691827	0.00011869
6.154522613	-0.009859748	0.000137301
6.192211055	-0.010013661	0.000160321
6.229899497	-0.010139929	0.000188008
6.26758794	-0.010263945	0.000208216
6.305276382	-0.01041863	0.000214596
6.342964824	-0.010592945	0.00020979
6.380653266	-0.010761299	0.000199661
6.418341709	-0.010916236	0.000188365
6.456030151	-0.011065315	0.000176073
6.493718593	-0.011224598	0.000167974
6.531407035	-0.011390228	0.000163425
6.569095477	-0.011539063	0.000149319
6.60678392	-0.011674827	0.000124987
6.644472362	-0.011818528	0.000106652
6.682160804	-0.011980882	0.000102716
6.719849246	-0.012158512	0.000104046
6.757537688	-0.012333843	9.94608E-05
6.795226131	-0.012506622	0.000088815
6.832914573	-0.012665071	7.91376E-05
6.870603015	-0.012802756	0.000075275
6.908291457	-0.012943709	7.71468E-05
6.945979899	-0.013108228	8.15172E-05
6.983668342	-0.013289591	8.49898E-05
7.021356784	-0.013457512	9.21582E-05
7.059045226	-0.013618	0.00010481
7.096733668	-0.013770764	0.000120484
7.134422111	-0.01392752	0.000139067
7.172110553	-0.014108488	0.000159146
7.209798995	-0.014295567	0.000177505
7.247487437	-0.014464394	0.000194287
7.285175879	-0.014646039	0.000219428
7.322864322	-0.014852425	0.000252517
7.360552764	-0.015058764	0.000280948

7.398241206	-0.01524011	0.000293399
7.435929648	-0.015403291	0.000286404
7.47361809	-0.015584031	0.000268349
7.511306533	-0.015767551	0.000241465
7.548994975	-0.015953496	0.000208243
7.586683417	-0.016133047	0.000178218
7.624371859	-0.016284142	0.00015387
7.662060302	-0.016430606	0.000132322
7.699748744	-0.016612134	0.000117838
7.737437186	-0.016806693	0.000110231
7.775125628	-0.016994724	0.000110041
7.81281407	-0.017166205	0.000113484
7.850502513	-0.017332874	0.000122181
7.888190955	-0.017510331	0.000148077
7.925879397	-0.017704433	0.000186093
7.963567839	-0.017908858	0.000218838
8.001256281	-0.018106992	0.000230672
8.038944724	-0.018292016	0.00021903
8.076633166	-0.018466197	0.000208574
8.114321608	-0.01861848	0.000205025
8.15201005	-0.018792047	0.000192118
8.189698492	-0.018988386	0.000170447
8.227386935	-0.01920578	0.00015311
8.265075377	-0.019394457	0.000144372
8.302763819	-0.019573921	0.000145226
8.340452261	-0.01975852	0.000150945
8.378140704	-0.019976882	0.000156328
8.415829146	-0.020190323	0.000155099
8.453517588	-0.020387882	0.000143862
8.49120603	-0.020589709	0.000130179
8.528894472	-0.020789858	0.000121028
8.566582915	-0.02098222	0.000116588
8.604271357	-0.021171937	0.000112487
8.641959799	-0.021365732	9.79828E-05
8.679648241	-0.021563378	0.000072341
8.717336683	-0.021750622	0.00005308
8.755025126	-0.021933441	0.000047762

8.792713568	-0.022130567	4.53152E-05
8.83040201	-0.022332984	4.20306E-05
8.868090452	-0.022522638	4.28466E-05
8.905778894	-0.022710551	5.45002E-05
8.943467337	-0.022906244	7.87088E-05
8.981155779	-0.023101441	0.000101968
9.018844221	-0.023299504	0.000111281
9.056532663	-0.023503709	0.000108787
9.094221106	-0.023708717	0.000102049
9.131909548	-0.023900472	9.12118E-05
9.16959799	-0.024076472	7.32786E-05
9.207286432	-0.024269047	0.00005314
9.244974874	-0.024477189	3.55388E-05
9.282663317	-0.024677614	0.00001584
9.320351759	-0.024881016	-0.000005376
9.358040201	-0.025095661	-0.00001579
9.395728643	-0.025312551	-0.000007018
9.433417085	-0.025524402	0.000018008
9.471105528	-0.025725921	0.000049779
9.50879397	-0.025926071	8.32524E-05
9.546482412	-0.026130772	0.000120701
9.584170854	-0.026334102	0.000157873
9.621859296	-0.02654322	0.000185589
9.659547739	-0.026756906	0.000190787
9.697236181	-0.026969921	0.000168314
9.734924623	-0.027184409	0.000134657
9.772613065	-0.02740474	0.000108422
9.810301508	-0.027625252	9.21016E-05
9.84798995	-0.02783122	7.81916E-05
9.885678392	-0.028026102	0.00005932
9.923366834	-0.028206835	0.000038144
9.961055276	-0.028390055	0.000023896
9.998743719	-0.028593457	0.0000211
10.03643216	-0.028817803	0.0000226
10.0741206	-0.029053433	0.000027188
10.11180905	-0.029276843	3.75576E-05
10.14949749	-0.029483126	4.49448E-05

10.18718593	-0.029686535	3.82436E-05
10.22487437	-0.029904024	0.000033706
10.26256281	-0.030126787	0.00004658
10.30025126	-0.030337504	0.00006504
10.3379397	-0.030529315	0.0000635
10.37562814	-0.030733724	0.00005196
10.41331658	-0.030967409	5.96046E-05
10.45100503	-0.031180803	8.95084E-05
10.48869347	-0.031377945	0.000124869
10.52638191	-0.031595598	0.000153258
10.56407035	-0.031855165	0.0001702
10.60175879	-0.032114772	0.000173794
10.63944724	-0.032347189	0.00015907
10.67713568	-0.032551433	0.000128099
10.71482412	-0.032748929	9.33844E-05
10.75251256	-0.03294374	5.71166E-05
10.79020101	-0.03315763	0.000019936
10.82788945	-0.033392354	-0.00001212
10.86557789	-0.033618843	-0.0000359
10.90326633	-0.033815291	-4.89188E-05
10.94095477	-0.034012031	-0.000045992
10.97864322	-0.034227787	-0.000024248
11.01633166	-0.034446449	0.000009314
11.0540201	-0.034654717	0.00003868
11.09170854	-0.034868669	0.00005702
11.12939698	-0.035100126	0.0000721
11.16708543	-0.035333457	9.25204E-05
11.20477387	-0.035562929	0.000115683
11.24246231	-0.035798071	0.000125018
11.28015075	-0.036031969	0.000108127
11.3178392	-0.03625452	7.77724E-05
11.35552764	-0.036458008	0.000048184
11.39321608	-0.036654433	0.00001726
11.43090452	-0.036871756	-0.000012878
11.46859296	-0.037114409	-0.00003178
11.50628141	-0.037360157	-0.000040038
11.54396985	-0.037577811	-0.00004862

11.58165829	-0.037776126	-0.00005692
11.61934673	-0.037985276	-0.00005208
11.65703518	-0.038202764	-3.00374E-05
11.69472362	-0.038426063	0.000002604
11.73241206	-0.038655323	0.000039819
11.7701005	-0.03888926	0.000078121
11.80778894	-0.039119362	0.000113541
11.84547739	-0.039336433	0.000143712
11.88316583	-0.039542835	0.000169054
11.92085427	-0.039760079	0.000190407
11.95854271	-0.039988976	0.000201324
11.99623116	-0.040231339	0.000190407
12.0339196	-0.040469606	0.0001607
12.07160804	-0.040702598	0.000119037
12.10929648	-0.040921181	6.88308E-05
12.14698492	-0.041138583	1.71838E-05
12.18467337	-0.041361654	-0.00002716
12.22236181	-0.041605039	-5.99038E-05
12.26005025	-0.04183	-9.61934E-05
12.29773869	-0.042029764	-0.000141799
12.33542714	-0.042246772	-0.000180697
12.37311558	-0.042465433	-0.00018198
12.41080402	-0.042699685	-0.000143203
12.44849246	-0.042929843	-8.97528E-05
12.4861809	-0.043145354	-0.000036232
12.52386935	-0.043351732	0.000029714
12.56155779	-0.043555984	0.000139439
12.59924623	-0.043769606	0.000275178
12.63693467	-0.043998268	0.000431759
12.67462312	-0.04425811	0.000625011
12.71231156	-0.044525039	0.000858006
12.75	-0.044770315	0.00113509

APPENDIX B: DIC FOV 2 DATA

Table B.1. Load 1: Raw DIC Deflection and Strain Data for FOV 2

Distance x along the Beam (inches)	Average Deflection (inches)	Average ε_{xx} Strain (in/in)
11.25	-0.008006543	1.58868E-05
11.3178392	-0.008130079	5.89803E-06
11.38567839	-0.008198024	8.48114E-06
11.45351759	-0.008274299	2.59048E-05
11.52135678	-0.008359323	3.03781E-05
11.58919598	-0.008439071	3.21647E-05
11.65703518	-0.008542205	5.13541E-05
11.72487437	-0.008650425	6.42554E-05
11.79271357	-0.008749953	6.50742E-05
11.86055276	-0.008827669	5.52851E-05
11.92839196	-0.008916512	3.17136E-05
11.99623116	-0.009017283	-6.71971E-07
12.06407035	-0.009131606	-3.35994E-05
12.13190955	-0.00928248	-6.27572E-05
12.19974874	-0.009404024	-8.51975E-05
12.26758794	-0.009475291	-9.41017E-05
12.33542714	-0.009549496	-9.37429E-05
12.40326633	-0.009655669	-7.8809E-05
12.47110553	-0.009746039	-4.69566E-05
12.53894472	-0.009774835	-3.27377E-05
12.60678392	-0.009870252	-3.85396E-05
12.67462312	-0.009943976	-4.36814E-05
12.74246231	-0.010038504	-3.85244E-05
12.81030151	-0.010180898	-4.86338E-05
12.8781407	-0.010268953	-5.07045E-05

12.9459799	-0.010328913	-1.97401E-05
13.0138191	-0.010419732	1.76331E-05
13.08165829	-0.010521496	4.89738E-05
13.14949749	-0.010633646	6.18126E-05
13.21733668	-0.01071015	6.98828E-05
13.28517588	-0.010746685	5.74114E-05
13.35301508	-0.010841	3.53807E-05
13.42085427	-0.010948024	2.66335E-05
13.48869347	-0.011065031	1.20726E-05
13.55653266	-0.011153181	-2.11485E-06
13.62437186	-0.011208213	2.62212E-07
13.69221106	-0.011320331	1.1111E-05
13.76005025	-0.011431425	2.19237E-05
13.82788945	-0.011498992	2.48422E-05
13.89572864	-0.011577504	3.13085E-05
13.96356784	-0.011627031	4.97883E-05
14.03140704	-0.011729598	6.08063E-05
14.09924623	-0.011857882	6.24845E-05
14.16708543	-0.011942055	7.15994E-05
14.23492462	-0.012029165	7.33922E-05
14.30276382	-0.012120827	5.74814E-05
14.37060302	-0.012221472	3.5504E-05
14.43844221	-0.012308228	1.95333E-05
14.50628141	-0.012361661	4.29809E-06
14.5741206	-0.012441693	-8.50574E-06
14.6419598	-0.012534244	5.77391E-06
14.70979899	-0.012629882	2.16313E-05
14.77763819	-0.012744197	2.34285E-05
14.84547739	-0.012863764	1.66635E-05
14.91331658	-0.012932268	1.45293E-05
14.98115578	-0.013008244	4.62949E-06
15.04899497	-0.013081843	-2.27071E-05
15.11683417	-0.013176898	-4.32153E-05
15.18467337	-0.013305472	-5.09835E-05
15.25251256	-0.013349024	-5.43167E-05
15.32035176	-0.01352337	-4.73763E-05
15.38819095	-0.01361863	-3.59585E-05

15.45603015	-0.013645858	-1.73525E-05
15.52386935	-0.013712496	-2.71127E-06
15.59170854	-0.013766937	2.15823E-06
15.65954774	-0.013859858	3.80067E-06
15.72738693	-0.013989276	-1.90754E-06
15.79522613	-0.014071598	-7.6117E-06
15.86306533	-0.014147496	-5.45744E-06
15.93090452	-0.01423211	1.99259E-05
15.99874372	-0.014312874	5.28492E-05
16.06658291	-0.014396079	8.15304E-05
16.13442211	-0.014519142	9.10052E-05
16.20226131	-0.014622213	8.51524E-05
16.2701005	-0.014675606	7.00414E-05
16.3379397	-0.014751315	2.2569E-05
16.40577889	-0.01488374	-2.8138E-05
16.47361809	-0.014968693	-5.88511E-05
16.54145729	-0.015009906	-8.76863E-05
16.60929648	-0.015086031	-9.51153E-05
16.67713568	-0.015181669	-9.2634E-05
16.74497487	-0.015310008	-8.1357E-05
16.81281407	-0.015375165	-7.89382E-05
16.88065327	-0.015450874	-7.62683E-05
16.94849246	-0.015516992	-4.53201E-05
17.01633166	-0.015580126	-3.02806E-05
17.08417085	-0.015679165	-2.22579E-05
17.15201005	-0.015743638	1.28243E-05
17.21984925	-0.015802591	4.77722E-05
17.28768844	-0.015881268	8.01067E-05
17.35552764	-0.015973181	8.85061E-05
17.42336683	-0.016049937	0.000101754
17.49120603	-0.016157677	0.000118779
17.55904523	-0.016230394	0.000108986
17.62688442	-0.016296197	9.42683E-05
17.69472362	-0.016372882	7.58285E-05
17.76256281	-0.016446244	6.35037E-05
17.83040201	-0.01652115	6.69697E-05
17.89824121	-0.01659989	5.85038E-05

17.9660804	-0.016667063	6.33857E-05
18.0339196	-0.016728402	6.36883E-05
18.10175879	-0.016792031	5.08575E-05
18.16959799	-0.016826701	5.37589E-05
18.23743719	-0.016899496	4.47719E-05
18.30527638	-0.016989969	2.96296E-05
18.37311558	-0.017044016	2.28415E-05
18.44095477	-0.017124205	1.67366E-05
18.50879397	-0.017220819	1.33597E-06
18.57663317	-0.017301	-2.52606E-05
18.64447236	-0.017358976	-4.04954E-05
18.71231156	-0.017400748	-5.2663E-05
18.78015075	-0.017500472	-6.53414E-05
18.84798995	-0.017600535	-6.53754E-05
18.91582915	-0.017651386	-6.99295E-05
18.98366834	-0.017720425	-7.64602E-05
19.05150754	-0.017778819	-7.31689E-05
19.11934673	-0.017844953	-6.38404E-05
19.18718593	-0.01791715	-6.26065E-05
19.25502513	-0.017993441	-7.31211E-05
19.32286432	-0.018055756	-7.28045E-05
19.39070352	-0.018112795	-6.2226E-05
19.45854271	-0.01819515	-5.33974E-05
19.52638191	-0.018263661	-5.02561E-05
19.59422111	-0.018316244	-5.74158E-05
19.6620603	-0.01835363	-6.58579E-05
19.7298995	-0.018407654	-5.22082E-05
19.79773869	-0.01846085	-3.00735E-05
19.86557789	-0.018536921	-3.70912E-07
19.93341709	-0.018611331	1.91876E-05
20.00125628	-0.01864089	2.31686E-05
20.06909548	-0.018709402	1.8473E-05
20.13693467	-0.018793205	5.99328E-06
20.20477387	-0.018838299	-2.02106E-05
20.27261307	-0.018914307	-6.44863E-05
20.34045226	-0.018976024	-0.000108493
20.40829146	-0.019011811	-0.000122666

20.47613065	-0.019074709	-0.000119584
20.54396985	-0.019151118	-9.63663E-05
20.61180905	-0.019162835	-4.70279E-05
20.67964824	-0.019191024	-3.17978E-06
20.74748744	-0.019298638	3.0774E-05
20.81532663	-0.019368024	5.79228E-05
20.88316583	-0.019398709	6.7565E-05
20.95100503	-0.019465394	6.12451E-05
21.01884422	-0.019517598	3.10521E-05
21.08668342	-0.01957089	-5.69534E-06
21.15452261	-0.019625984	-3.37286E-05
21.22236181	-0.019665142	-4.43448E-05
21.29020101	-0.019716323	-4.64897E-05
21.3580402	-0.019752205	-4.92587E-05
21.4258794	-0.019802732	-4.4256E-05
21.49371859	-0.019834024	-2.60043E-05
21.56155779	-0.019889661	-2.4041E-05
21.62939698	-0.019901669	-2.16947E-05
21.69723618	-0.019900701	-9.72326E-06
21.76507538	-0.020004472	-2.49753E-05
21.83291457	-0.020089094	-4.98242E-05
21.90075377	-0.020106858	-5.5294E-05
21.96859296	-0.020152276	-6.15528E-05
22.03643216	-0.020174646	-8.30384E-05
22.10427136	-0.02022763	-0.000102472
22.17211055	-0.020304134	-0.000100325
22.23994975	-0.020330425	-9.95147E-05
22.30778894	-0.020363425	-9.98993E-05
22.37562814	-0.020378811	-7.69709E-05
22.44346734	-0.020417677	-5.58795E-05
22.51130653	-0.020457173	-3.43704E-05
22.57914573	-0.020503969	-1.33428E-05
22.64698492	-0.020545354	7.57692E-06
22.71482412	-0.020556346	2.89675E-05
22.78266332	-0.020626575	1.60603E-05
22.85050251	-0.020704843	-1.70734E-05
22.91834171	-0.020715441	-3.19921E-05

22.9861809	-0.020755291	-2.97357E-05
23.0540201	-0.020777528	-2.22491E-05
23.1218593	-0.020801669	-1.79316E-05
23.18969849	-0.020834457	7.98094E-07
23.25753769	-0.020855874	3.30511E-05
23.32537688	-0.020850874	5.06141E-05
23.39321608	-0.020882331	5.72884E-05
23.46105528	-0.020899472	4.9847E-05
23.52889447	-0.02093174	1.59397E-05
23.59673367	-0.020987992	-3.19651E-05
23.66457286	-0.020989882	-8.03184E-05
23.73241206	-0.020979535	-8.8424E-05
23.80025126	-0.020955291	-8.65984E-05
23.86809045	-0.020990528	-9.84108E-05
23.93592965	-0.021046087	-8.22476E-05
24.00376884	-0.021048079	-5.25265E-05
24.07160804	-0.021044622	-3.59656E-05
24.13944724	-0.021079748	-3.76424E-05
24.20728643	-0.021125102	-5.44207E-05
24.27512563	-0.021152173	-6.52815E-05
24.34296482	-0.021181945	-6.23794E-05
24.41080402	-0.02117748	-4.90697E-05
24.47864322	-0.021139717	-3.4013E-05
24.54648241	-0.021164921	-1.72683E-05
24.61432161	-0.02119622	-8.35298E-06
24.6821608	-0.021218819	-2.53827E-05
24.75	-0.02120511	-8.30719E-05

Table B.2. Load 2: Raw DIC Deflection and Strain Data for FOV 2

Distance x along the Beam (inches)	Average Deflection (inches)	Average ε_{xx} Strain (in/in)
11.25	-0.019964205	-0.000272021
11.3178392	-0.020199756	-0.00014344
11.38567839	-0.020416102	-5.54978E-05
11.45351759	-0.020646346	1.68688E-05

11.52135678	-0.020835732	4.36463E-05
11.58919598	-0.021022142	6.30832E-05
11.65703518	-0.021234976	6.82392E-05
11.72487437	-0.021461772	6.46801E-05
11.79271357	-0.021673622	4.6291E-05
11.86055276	-0.021904134	8.44483E-06
11.92839196	-0.022139748	-2.33919E-05
11.99623116	-0.022342583	-5.35536E-05
12.06407035	-0.022531472	-6.46757E-05
12.13190955	-0.022789472	-6.06326E-05
12.19974874	-0.023033654	-6.81236E-05
12.26758794	-0.023214819	-6.52308E-05
12.33542714	-0.023390465	-7.54003E-05
12.40326633	-0.023637929	-9.33222E-05
12.47110553	-0.023876756	-8.42465E-05
12.53894472	-0.02401048	-0.000074214
12.60678392	-0.024238598	-7.11359E-05
12.67462312	-0.024498984	-6.20186E-05
12.74246231	-0.02470863	-2.775E-05
12.81030151	-0.024946559	-2.47372E-05
12.8781407	-0.025160354	-2.94521E-05
12.9459799	-0.025346882	-8.39044E-06
13.0138191	-0.025587898	1.81229E-05
13.08165829	-0.025853677	3.09049E-05
13.14949749	-0.026097307	4.0908E-05
13.21733668	-0.026266283	7.08907E-05
13.28517588	-0.026420882	7.38788E-05
13.35301508	-0.02663785	5.18905E-05
13.42085427	-0.026874827	0.000049121
13.48869347	-0.027138913	2.30277E-05
13.55653266	-0.027341835	5.21804E-06
13.62437186	-0.027505291	1.83115E-05
13.69221106	-0.027709024	3.63206E-05
13.76005025	-0.02794015	4.28002E-05
13.82788945	-0.028156142	3.51377E-05
13.89572864	-0.028328213	2.9196E-05
13.96356784	-0.028507898	2.18806E-05

14.03140704	-0.02874174	2.51383E-05
14.09924623	-0.028985173	3.2104E-05
14.16708543	-0.029183276	5.21435E-05
14.23492462	-0.029398339	7.3316E-05
14.30276382	-0.029614543	8.08943E-05
14.37060302	-0.029857339	7.78508E-05
14.43844221	-0.030061157	6.22427E-05
14.50628141	-0.030210079	2.46822E-05
14.5741206	-0.03043674	-1.46417E-05
14.6419598	-0.030674441	-3.52256E-05
14.70979899	-0.030888008	-3.04007E-05
14.77763819	-0.031119622	-3.12708E-05
14.84547739	-0.031362528	-4.03455E-05
14.91331658	-0.031555276	-1.62798E-05
14.98115578	-0.031748339	5.581E-08
15.04899497	-0.031947764	-1.92794E-05
15.11683417	-0.032159244	-3.58009E-05
15.18467337	-0.032342866	-4.78453E-05
15.25251256	-0.032542606	-6.71389E-05
15.32035176	-0.032844276	-7.94299E-05
15.38819095	-0.033018496	-6.818E-05
15.45603015	-0.033183173	-4.60647E-05
15.52386935	-0.033388543	-3.64443E-05
15.59170854	-0.033557567	-2.99305E-05
15.65954774	-0.033762717	-1.0635E-05
15.72738693	-0.033984346	-1.90452E-06
15.79522613	-0.03416026	5.51518E-06
15.86306533	-0.034351142	1.37138E-05
15.93090452	-0.034568669	4.82829E-05
15.99874372	-0.03478263	7.7966E-05
16.06658291	-0.034949449	8.3427E-05
16.13442211	-0.035138669	6.96265E-05
16.20226131	-0.03534289	3.29513E-05
16.2701005	-0.035510071	-1.97153E-05
16.3379397	-0.035739197	-8.82802E-05
16.40577889	-0.035962724	-0.000147452
16.47361809	-0.036143181	-0.000156882

16.54145729	-0.036353134	-0.000171817
16.60929648	-0.036528449	-0.000157807
16.67713568	-0.036720709	-0.000128156
16.74497487	-0.036965378	-0.000101198
16.81281407	-0.037116709	-7.31284E-05
16.88065327	-0.037313087	-4.9706E-05
16.94849246	-0.037492236	-1.82923E-05
17.01633166	-0.03765748	-1.47877E-05
17.08417085	-0.037856205	-2.49637E-05
17.15201005	-0.038013772	-1.60759E-06
17.21984925	-0.038208331	1.88203E-05
17.28768844	-0.038379465	4.91249E-05
17.35552764	-0.038579882	5.74816E-05
17.42336683	-0.038758795	6.98746E-05
17.49120603	-0.038932134	9.39293E-05
17.55904523	-0.039117685	8.34787E-05
17.62688442	-0.039310827	6.44936E-05
17.69472362	-0.039515906	4.35018E-05
17.76256281	-0.039672992	1.90473E-05
17.83040201	-0.039825669	1.22474E-05
17.89824121	-0.039989843	5.47453E-06
17.9660804	-0.040151417	1.79853E-05
18.0339196	-0.040307323	2.2031E-05
18.10175879	-0.040487165	1.27807E-05
18.16959799	-0.040647323	1.21286E-05
18.23743719	-0.040825197	-6.9698E-06
18.30527638	-0.041001102	-2.95773E-05
18.37311558	-0.041136693	-3.26407E-05
18.44095477	-0.041331024	-3.46274E-05
18.50879397	-0.04149378	-3.73797E-05
18.57663317	-0.041655118	-4.03858E-05
18.64447236	-0.041839528	-3.31372E-05
18.71231156	-0.041992205	-3.76081E-05
18.78015075	-0.042194094	-5.69434E-05
18.84798995	-0.042392835	-7.60379E-05
18.91582915	-0.042525039	-0.000104042
18.98366834	-0.042666142	-0.000125157

19.05150754	-0.042788819	-0.000128304
19.11934673	-0.042955512	-0.000125327
19.18718593	-0.043142126	-0.000118544
19.25502513	-0.043306378	-0.000111658
19.32286432	-0.043453543	-0.000101303
19.39070352	-0.043604882	-8.68252E-05
19.45854271	-0.043773071	-7.96133E-05
19.52638191	-0.043895118	-7.98737E-05
19.59422111	-0.044025827	-9.10486E-05
19.6620603	-0.044160079	-9.89331E-05
19.7298995	-0.044305197	-9.17205E-05
19.79773869	-0.044437402	-8.48434E-05
19.86557789	-0.044575591	-6.85389E-05
19.93341709	-0.044736063	-5.16969E-05
20.00125628	-0.04485874	-5.28049E-05
20.06909548	-0.04499748	-5.52758E-05
20.13693467	-0.045145512	-6.69912E-05
20.20477387	-0.045264567	-8.29494E-05
20.27261307	-0.045401732	-0.000103013
20.34045226	-0.045526142	-0.000124093
20.40829146	-0.045647795	-0.000123027
20.47613065	-0.045791654	-0.000122888
20.54396985	-0.045940472	-0.000104494
20.61180905	-0.046024488	-7.25165E-05
20.67964824	-0.046140315	-5.46547E-05
20.74748744	-0.046308898	-4.42399E-05
20.81532663	-0.046441417	-3.77915E-05
20.88316583	-0.046546299	-4.03812E-05
20.95100503	-0.04667189	-4.07754E-05
21.01884422	-0.04677315	-5.05854E-05
21.08668342	-0.046891732	-6.16691E-05
21.15452261	-0.04702874	-7.28062E-05
21.22236181	-0.04713874	-6.30997E-05
21.29020101	-0.047252913	-6.53395E-05
21.3580402	-0.047348031	-9.38853E-05
21.4258794	-0.047466772	-0.000115259
21.49371859	-0.047572047	-0.000109578

21.56155779	-0.047684961	-0.000109321
21.62939698	-0.047759843	-0.000104226
21.69723618	-0.047820866	-7.54846E-05
21.76507538	-0.047968031	-7.31337E-05
21.83291457	-0.048104803	-9.83818E-05
21.90075377	-0.04819063	-0.000115737
21.96859296	-0.048299528	-0.000131359
22.03643216	-0.048363228	-0.000158255
22.10427136	-0.048440472	-0.00018772
22.17211055	-0.048562756	-0.000180701
22.23994975	-0.048643858	-0.000161241
22.30778894	-0.048729134	-0.000150597
22.37562814	-0.048805906	-0.000118959
22.44346734	-0.048896535	-0.000101983
22.51130653	-0.048990551	-9.56832E-05
22.57914573	-0.049095354	-8.42037E-05
22.64698492	-0.049169213	-6.67544E-05
22.71482412	-0.049231654	-4.59887E-05
22.78266332	-0.049350157	-4.32597E-05
22.85050251	-0.049475748	-5.74902E-05
22.91834171	-0.049547638	-6.79953E-05
22.9861809	-0.049592126	-7.17454E-05
23.0540201	-0.049660866	-7.17635E-05
23.1218593	-0.049740551	-7.55813E-05
23.18969849	-0.049779213	-7.84214E-05
23.25753769	-0.049842362	-7.17246E-05
23.32537688	-0.049896535	-6.56398E-05
23.39321608	-0.049950866	-6.21506E-05
23.46105528	-0.049992992	-5.70636E-05
23.52889447	-0.050041575	-6.37249E-05
23.59673367	-0.050132047	-9.49386E-05
23.66457286	-0.050171969	-0.000128967
23.73241206	-0.050201102	-0.000133725
23.80025126	-0.050210945	-0.000140051
23.86809045	-0.050264016	-0.000167343
23.93592965	-0.050320315	-0.000181063
24.00376884	-0.050348898	-0.000176683

24.07160804	-0.050394252	-0.000172675
24.13944724	-0.05044	-0.000164504
24.20728643	-0.050512677	-0.00016938
24.27512563	-0.050565039	-0.000170353
24.34296482	-0.05059622	-0.000151957
24.41080402	-0.05061622	-0.000130425
24.47864322	-0.050605827	-0.00010949
24.54648241	-0.050634409	-8.65804E-05
24.61432161	-0.050687874	-0.000068772
24.6821608	-0.050720472	-5.3294E-05
24.75	-0.050689055	-6.17464E-05

Table B.3. Load 3: Raw DIC Deflection and Strain Data for FOV 2

Distance x along the Beam (inches)	Average Deflection (inches)	Average ε_{xx} Strain (in/in)
11.25	-0.040544016	-0.000222029
11.3178392	-0.041024646	-9.0607E-05
11.38567839	-0.041407638	-1.51813E-05
11.45351759	-0.041807638	5.11284E-05
11.52135678	-0.042240472	7.63505E-05
11.58919598	-0.042665591	9.05878E-05
11.65703518	-0.043110866	9.67692E-05
11.72487437	-0.043526693	0.000101971
11.79271357	-0.043935197	9.74349E-05
11.86055276	-0.044366142	6.60485E-05
11.92839196	-0.044791811	2.7108E-05
11.99623116	-0.045200236	-2.87801E-05
12.06407035	-0.045608425	-6.08007E-05
12.13190955	-0.046075354	-7.47398E-05
12.19974874	-0.046550866	-7.2339E-05
12.26758794	-0.04693685	-5.30669E-05
12.33542714	-0.04731126	-5.1679E-05
12.40326633	-0.047758346	-5.01113E-05
12.47110553	-0.048185906	-2.25613E-05
12.53894472	-0.048520157	-2.07299E-05

12.60678392	-0.048941969	-3.65003E-05
12.67462312	-0.049369134	-4.6291E-05
12.74246231	-0.049822362	-2.37909E-05
12.81030151	-0.050253937	-2.97158E-05
12.8781407	-0.050656693	-2.72255E-05
12.9459799	-0.051058661	7.5176E-07
13.0138191	-0.05150315	1.91114E-05
13.08165829	-0.051954173	1.72207E-05
13.14949749	-0.052416614	5.07365E-06
13.21733668	-0.052813543	3.19867E-05
13.28517588	-0.053160787	5.09791E-05
13.35301508	-0.053583228	6.85023E-05
13.42085427	-0.054023622	9.55416E-05
13.48869347	-0.054462047	8.3874E-05
13.55653266	-0.054893858	7.73951E-05
13.62437186	-0.055264961	7.12902E-05
13.69221106	-0.055674961	4.94639E-05
13.76005025	-0.056148583	2.46045E-05
13.82788945	-0.056557795	-5.10597E-06
13.89572864	-0.056907165	-0.000019076
13.96356784	-0.057287717	-1.99176E-05
14.03140704	-0.057696535	-1.39947E-05
14.09924623	-0.058113701	-1.57083E-05
14.16708543	-0.058534173	-1.41535E-05
14.23492462	-0.058980315	-6.36438E-07
14.30276382	-0.059386299	1.26379E-05
14.37060302	-0.059858189	2.26382E-05
14.43844221	-0.060246378	2.76955E-05
14.50628141	-0.060552913	2.43147E-05
14.5741206	-0.06093685	6.51297E-06
14.6419598	-0.061398819	-1.43467E-06
14.70979899	-0.06180748	7.45006E-06
14.77763819	-0.062219449	-1.50068E-05
14.84547739	-0.062652992	-5.39726E-05
14.91331658	-0.063028504	-4.88897E-05
14.98115578	-0.063384646	-3.97807E-05
15.04899497	-0.063775039	-5.63403E-05

15.11683417	-0.064236614	-7.01093E-05
15.18467337	-0.064619685	-7.31909E-05
15.25251256	-0.064968898	-9.17786E-05
15.32035176	-0.065492835	-0.000129152
15.38819095	-0.065891024	-0.000134538
15.45603015	-0.066252756	-0.000119948
15.52386935	-0.06661685	-0.000126972
15.59170854	-0.066952362	-0.000116449
15.65954774	-0.067344724	-9.46966E-05
15.72738693	-0.067725827	-7.19912E-05
15.79522613	-0.068112205	-4.3996E-05
15.86306533	-0.068493701	-2.87413E-05
15.93090452	-0.068875748	7.91678E-06
15.99874372	-0.069281575	3.70501E-05
16.06658291	-0.06966252	4.10735E-05
16.13442211	-0.070045906	2.49573E-05
16.20226131	-0.07042063	-1.92773E-05
16.2701005	-0.070808976	-7.01283E-05
16.3379397	-0.071181102	-0.000134729
16.40577889	-0.071569055	-0.000200421
16.47361809	-0.071933622	-0.000196205
16.54145729	-0.072317638	-0.000173801
16.60929648	-0.072677795	-0.000130124
16.67713568	-0.073046929	-8.30379E-05
16.74497487	-0.073442441	-4.24805E-05
16.81281407	-0.073771654	-3.29735E-05
16.88065327	-0.074140709	-4.17164E-05
16.94849246	-0.074489606	-4.64179E-05
17.01633166	-0.074852205	-6.76542E-05
17.08417085	-0.075217402	-8.65277E-05
17.15201005	-0.075525748	-6.33437E-05
17.21984925	-0.07588811	-3.85236E-05
17.28768844	-0.076264173	-7.2133E-06
17.35552764	-0.07664748	-8.51414E-07
17.42336683	-0.076963622	1.57144E-05
17.49120603	-0.077327323	3.9414E-05
17.55904523	-0.077660866	2.61907E-05

17.62688442	-0.078008504	1.3201E-05
17.69472362	-0.078367323	-9.28489E-06
17.76256281	-0.078684409	-3.42548E-05
17.83040201	-0.079020472	-3.77125E-05
17.89824121	-0.079364961	-5.29323E-05
17.9660804	-0.079670787	-5.82959E-05
18.0339196	-0.079984016	-6.05982E-05
18.10175879	-0.080331496	-6.01752E-05
18.16959799	-0.080637795	-4.40942E-05
18.23743719	-0.080962126	-4.56544E-05
18.30527638	-0.081297874	-5.20699E-05
18.37311558	-0.081630709	-5.20333E-05
18.44095477	-0.081973228	-6.07127E-05
18.50879397	-0.082271496	-8.18045E-05
18.57663317	-0.082590236	-0.000110752
18.64447236	-0.082946063	-0.000127135
18.71231156	-0.083242205	-0.000142549
18.78015075	-0.083537008	-0.000155601
18.84798995	-0.083872362	-0.000162325
18.91582915	-0.084159291	-0.00016978
18.98366834	-0.084439764	-0.000169822
19.05150754	-0.084705118	-0.0001701
19.11934673	-0.085001496	-0.000167638
19.18718593	-0.085344961	-0.000169111
19.25502513	-0.08567811	-0.000186707
19.32286432	-0.085962047	-0.000196558
19.39070352	-0.086212441	-0.000188198
19.45854271	-0.086515433	-0.000187556
19.52638191	-0.086795276	-0.000188013
19.59422111	-0.087076535	-0.000187214
19.6620603	-0.087375354	-0.000183166
19.7298995	-0.087668661	-0.000179658
19.79773869	-0.087917008	-0.000183191
19.86557789	-0.088158425	-0.000172396
19.93341709	-0.088457874	-0.000152201
20.00125628	-0.088710472	-0.000150758
20.06909548	-0.088954409	-0.000130118

20.13693467	-0.089218661	-0.000122047
20.20477387	-0.089464803	-0.000128547
20.27261307	-0.089761339	-0.000141775
20.34045226	-0.090022992	-0.000168765
20.40829146	-0.090249528	-0.000191677
20.47613065	-0.090500551	-0.000206657
20.54396985	-0.090767559	-0.000210537
20.61180905	-0.090990709	-0.000182716
20.67964824	-0.091218189	-0.00015182
20.74748744	-0.091480709	-0.000124577
20.81532663	-0.091733858	-0.000119084
20.88316583	-0.091961181	-0.000124772
20.95100503	-0.092205276	-0.000122891
21.01884422	-0.092426929	-0.000135624
21.08668342	-0.092659291	-0.000157017
21.15452261	-0.092909843	-0.00016187
21.22236181	-0.093110551	-0.000145365
21.29020101	-0.093308661	-0.000141485
21.3580402	-0.093512756	-0.000158132
21.4258794	-0.093735512	-0.000163531
21.49371859	-0.093923858	-0.00015424
21.56155779	-0.094145748	-0.00016811
21.62939698	-0.09433	-0.000172289
21.69723618	-0.094474724	-0.00015452
21.76507538	-0.094699134	-0.000161115
21.83291457	-0.094925276	-0.000190306
21.90075377	-0.095075984	-0.000208172
21.96859296	-0.095277008	-0.000224969
22.03643216	-0.09545126	-0.000259838
22.10427136	-0.095604646	-0.000294926
22.17211055	-0.095820315	-0.000289588
22.23994975	-0.095994882	-0.000279827
22.30778894	-0.09615189	-0.000286844
22.37562814	-0.09633189	-0.000276651
22.44346734	-0.096494016	-0.000262631
22.51130653	-0.096648189	-0.000238414
22.57914573	-0.09680622	-0.000210668

22.64698492	-0.096974488	-0.000172958
22.71482412	-0.097148425	-0.000139861
22.78266332	-0.0973	-0.000145079
22.85050251	-0.097450945	-0.000175694
22.91834171	-0.097600472	-0.000199538
22.9861809	-0.097761339	-0.000215969
23.0540201	-0.097906142	-0.000234633
23.1218593	-0.098060394	-0.000254368
23.18969849	-0.098170787	-0.000247896
23.25753769	-0.098279213	-0.000226787
23.32537688	-0.098362205	-0.000209538
23.39321608	-0.098454567	-0.000180706
23.46105528	-0.098556299	-0.000157853
23.52889447	-0.098681181	-0.000151607
23.59673367	-0.098850394	-0.000168086
23.66457286	-0.098920157	-0.000199909
23.73241206	-0.098972205	-0.000210049
23.80025126	-0.099048425	-0.000223714
23.86809045	-0.099167795	-0.000264249
23.93592965	-0.099307008	-0.00028731
24.00376884	-0.099392677	-0.000288788
24.07160804	-0.099448976	-0.000275702
24.13944724	-0.099547087	-0.000259014
24.20728643	-0.099629685	-0.00026561
24.27512563	-0.099705354	-0.00027417
24.34296482	-0.099761496	-0.000274838
24.41080402	-0.099806457	-0.000273841
24.47864322	-0.099839528	-0.000269233
24.54648241	-0.099899685	-0.000262975
24.61432161	-0.099989685	-0.000268441
24.6821608	-0.100067559	-0.000279152
24.75	-0.100050945	-0.000304097

APPENDIX C: ANSYS DATA

Table C.1. Load 1: FE Model Deflection and Strain Data

Distance x along the Beam (inches)	Deflection (inches)	Ɛxx Strain (in/in)
0	0	0.0001147
0.975961538	-0.00016855	0.00011243
1.951923077	-0.00051062	0.00010221
2.927884615	-0.0010414	0.000092748
3.903846154	-0.0017471	0.000083309
4.879807692	-0.0026109	0.000074017
5.855769231	-0.0036154	0.000064758
6.831730769	-0.0047432	0.000055517
7.807692308	-0.0059766	0.000046281
8.783653846	-0.0072983	0.000037046
9.759615385	-0.0086905	0.000027811
10.73557692	-0.010136	0.000018575
11.71153846	-0.011616	9.3395E-06
12.6875	-0.013115	1.0371E-07
13.66346154	-0.014614	-9.1322E-06
14.63942308	-0.016095	-0.000018368
15.61538462	-0.017542	-0.000027604
16.59134615	-0.018936	-0.00003684
17.56730769	-0.02026	-0.000046075
18.54326923	-0.021496	-0.00005531
19.51923077	-0.022627	-0.000064546
20.49519231	-0.023635	-0.000073787
21.47115385	-0.024503	-0.000083063
22.44711538	-0.025213	-0.000092416
23.42307692	-0.025747	-0.00010198
24.39903846	-0.026085	-0.00011109

25.375	-0.026206	-0.00012197
26.35096154	-0.000068922	0.00011356
27.32692308	-0.00031692	0.00010732
28.30288462	-0.00075402	0.000097477
29.27884615	-0.001374	0.000088028
30.25480769	-0.0021607	0.000078663
31.23076923	-0.0030969	0.000069388
32.20673077	-0.0041652	0.000060138
33.18269231	-0.0053479	0.000050899
34.15865385	-0.0066276	0.000041663
35.13461538	-0.0079867	0.000032428
36.11057692	-0.0094076	0.000023193
37.08653846	-0.010873	0.000013957
38.0625	-0.012365	4.7216E-06
39.03846154	-0.013865	-4.5143E-06
40.01442308	-0.015358	-0.00001375
40.99038462	-0.016824	-0.000022986
41.96634615	-0.018246	-0.000032222
42.94230769	-0.019607	-0.000041457
43.91826923	-0.02089	-0.000050692
44.89423077	-0.022076	-0.000059928
45.87019231	-0.023148	-0.000069166
46.84615385	-0.024088	-0.000078425
47.82211538	-0.024879	-0.00008774
48.79807692	-0.025503	-0.000097199
49.77403846	-0.025941	-0.00010654
50.75	-0.026174	-0.00011653

Table C.2. Load 2: FE Model Deflection and Strain Data

Distance x along the Beam (inches)	Deflection (inches)	ε_{xx} Strain (mm)
0	0	0.00025803
0.975961538	-0.0003792	0.00025294
1.951923077	-0.0011488	0.00022994
2.927884615	-0.0023428	0.00020866
3.903846154	-0.0039305	0.00018742

4.879807692	-0.0058738	0.00016652
5.855769231	-0.0081337	0.00014569
6.831730769	-0.010671	0.0001249
7.807692308	-0.013446	0.00010412
8.783653846	-0.016419	0.000083343
9.759615385	-0.019551	0.000062566
10.73557692	-0.022803	0.000041789
11.71153846	-0.026134	0.000021011
12.6875	-0.029505	2.3331E-07
13.66346154	-0.032877	-0.000020545
14.63942308	-0.036209	-0.000041323
15.61538462	-0.039464	-0.000062102
16.59134615	-0.0426	-0.000082879
17.56730769	-0.045579	-0.00010366
18.54326923	-0.04836	-0.00012443
19.51923077	-0.050905	-0.00014521
20.49519231	-0.053173	-0.000166
21.47115385	-0.055126	-0.00018687
22.44711538	-0.056723	-0.00020791
23.42307692	-0.057923	-0.00022943
24.39903846	-0.058684	-0.00024992
25.375	-0.058956	-0.00027439
26.35096154	-0.00015506	0.00025549
27.32692308	-0.00071299	0.00024144
28.30288462	-0.0016963	0.0002193
29.27884615	-0.0030911	0.00019804
30.25480769	-0.004861	0.00017697
31.23076923	-0.0069672	0.0001561
32.20673077	-0.0093705	0.00013529
33.18269231	-0.012031	0.00011451
34.15865385	-0.01491	0.000093731
35.13461538	-0.017968	0.000072955
36.11057692	-0.021165	0.000052178
37.08653846	-0.024461	0.0000314
38.0625	-0.027817	0.000010622
39.03846154	-0.031193	-0.000010156
40.01442308	-0.03455	-0.000030934

40.99038462	-0.037849	-0.000051713
41.96634615	-0.041049	-0.00007249
42.94230769	-0.044111	-0.000093268
43.91826923	-0.046996	-0.00011404
44.89423077	-0.049664	-0.00013482
45.87019231	-0.052076	-0.00015561
46.84615385	-0.054191	-0.00017644
47.82211538	-0.055971	-0.00019739
48.79807692	-0.057375	-0.00021867
49.77403846	-0.058361	-0.00023968
50.75	-0.058886	-0.00026216

Table C.3. Load 3: FE Model Deflection and Strain Data

Distance x along the Beam (inches)	Deflection (inches)	ε_{xx} Strain (in/in)
0	0	0.00047306
0.975961538	-0.0006952	0.00046372
1.951923077	-0.0021061	0.00042155
2.927884615	-0.0042951	0.00038254
3.903846154	-0.0072059	0.00034361
4.879807692	-0.010769	0.00030529
5.855769231	-0.014912	0.0002671
6.831730769	-0.019563	0.00022898
7.807692308	-0.024651	0.00019089
8.783653846	-0.030102	0.0001528
9.759615385	-0.035844	0.00011471
10.73557692	-0.041805	0.000076614
11.71153846	-0.047912	0.000038521
12.6875	-0.054093	4.2774E-07
13.66346154	-0.060274	-0.000037666
14.63942308	-0.066384	-0.00007576
15.61538462	-0.072351	-0.00011385
16.59134615	-0.0781	-0.00015195
17.56730769	-0.083561	-0.00019004
18.54326923	-0.08866	-0.00022813
19.51923077	-0.093326	-0.00026622

20.49519231	-0.097484	-0.00030433
21.47115385	-0.10106	-0.0003426
22.44711538	-0.10399	-0.00038117
23.42307692	-0.10619	-0.00042063
24.39903846	-0.10759	-0.0004582
25.375	-0.10809	-0.00050305
26.35096154	-0.00028427	0.00046839
27.32692308	-0.0013072	0.00044264
28.30288462	-0.00311	0.00040205
29.27884615	-0.0056671	0.00036307
30.25480769	-0.0089119	0.00032445
31.23076923	-0.012773	0.00028619
32.20673077	-0.017179	0.00024804
33.18269231	-0.022058	0.00020993
34.15865385	-0.027336	0.00017184
35.13461538	-0.032941	0.00013375
36.11057692	-0.038802	0.00009566
37.08653846	-0.044845	0.000057567
38.0625	-0.050998	0.000019474
39.03846154	-0.057188	-0.000018619
40.01442308	-0.063343	-0.000056713
40.99038462	-0.06939	-0.000094807
41.96634615	-0.075257	-0.0001329
42.94230769	-0.080871	-0.00017099
43.91826923	-0.08616	-0.00020908
44.89423077	-0.091052	-0.00024717
45.87019231	-0.095473	-0.00028528
46.84615385	-0.099351	-0.00032347
47.82211538	-0.10261	-0.00036188
48.79807692	-0.10519	-0.0004009
49.77403846	-0.107	-0.00043941
50.75	-0.10796	-0.00048062

APPENDIX D: ANALYTICAL DATA

Table D.1. Load 1: Analytical Deflection and Strain Data

Distance x along the Beam (inches)	Deflection (inches)	ε_{xx} Strain (in/in)
0	0	0.000104104
0.975961538	-0.000109937	9.6096E-05
1.951923077	-0.000428175	8.8088E-05
2.927884615	-0.000937357	8.008E-05
3.903846154	-0.001620123	7.2072E-05
4.879807692	-0.002459115	6.4064E-05
5.855769231	-0.003436975	5.60559E-05
6.831730769	-0.004536344	4.80479E-05
7.807692308	-0.005739864	4.00399E-05
8.783653846	-0.007030176	3.20319E-05
9.759615385	-0.008389922	2.40239E-05
10.73557692	-0.009801744	1.60159E-05
11.71153846	-0.011248282	8.0079E-06
12.6875	-0.012712179	-1.09375E-10
13.66346154	-0.014176076	-8.00812E-06
14.63942308	-0.015622614	-1.60161E-05
15.61538462	-0.017034436	-2.40241E-05
16.59134615	-0.018394182	-3.20321E-05
17.56730769	-0.019684494	-4.00402E-05
18.54326923	-0.020888014	-4.80482E-05
19.51923077	-0.021987383	-5.60562E-05
20.49519231	-0.022965243	-6.40642E-05
21.47115385	-0.023804235	-7.20722E-05
22.44711538	-0.024487001	-8.00802E-05
23.42307692	-0.024996183	-8.80882E-05
24.39903846	-0.025314421	-9.60962E-05

25.375	-0.025424358	-0.000104104

Table D.2. Load 2: Analytical Deflection and Strain Data

Distance x along the Beam (inches)	Deflection (inches)	ε_{xx} Strain (in/in)
0	0	0.000266527
0.975961538	-0.000247358	0.000246025
1.951923077	-0.000963395	0.000225523
2.927884615	-0.002109053	0.000205021
3.903846154	-0.003645277	0.000184519
4.879807692	-0.005533009	0.000164017
5.855769231	-0.007733194	0.000143515
6.831730769	-0.010206775	0.000123013
7.807692308	-0.012914694	0.00010251
8.783653846	-0.015817897	8.20084E-05
9.759615385	-0.018877325	6.15063E-05
10.73557692	-0.022053924	4.10042E-05
11.71153846	-0.025308635	2.05021E-05
12.6875	-0.028602403	0
13.66346154	-0.031896171	-2.05021E-05
14.63942308	-0.035150882	-4.10042E-05
15.61538462	-0.03832748	-6.15063E-05
16.59134615	-0.041386909	-8.20084E-05
17.56730769	-0.044290111	-0.00010251
18.54326923	-0.046998031	-0.000123013
19.51923077	-0.049471611	-0.000143515
20.49519231	-0.051671796	-0.000164017
21.47115385	-0.053559529	-0.000184519
22.44711538	-0.055095753	-0.000205021
23.42307692	-0.056241411	-0.000225523
24.39903846	-0.056957447	-0.000246025
25.375	-0.057204805	-0.000266527

Table D.3. Load 3: Analytical Deflection and Strain Data

Distance x along the Beam (inches)	Deflection (inches)	ε_{xx} Strain (in/in)
0	0	0.000488633
0.975961538	-0.00045349	0.000451046
1.951923077	-0.001766223	0.000413459
2.927884615	-0.003866597	0.000375872
3.903846154	-0.006683007	0.000338285
4.879807692	-0.01014385	0.000300697
5.855769231	-0.014177522	0.00026311
6.831730769	-0.01871242	0.000225523
7.807692308	-0.02367694	0.000187936
8.783653846	-0.028999477	0.000150349
9.759615385	-0.03460843	0.000112762
10.73557692	-0.040432193	7.51744E-05
11.71153846	-0.046399164	3.75872E-05
12.6875	-0.052437738	0
13.66346154	-0.058476313	-3.75872E-05
14.63942308	-0.064443283	-7.51744E-05
15.61538462	-0.070267047	-0.000112762
16.59134615	-0.075875999	-0.000150349
17.56730769	-0.081198537	-0.000187936
18.54326923	-0.086163057	-0.000225523
19.51923077	-0.090697954	-0.00026311
20.49519231	-0.094731626	-0.000300697
21.47115385	-0.098192469	-0.000338285
22.44711538	-0.10100888	-0.000375872
23.42307692	-0.103109253	-0.000413459
24.39903846	-0.104421987	-0.000451046
25.375	-0.104875477	-0.000488633

REFERENCES

"Application Note AN-1701 Speckle Pattern Fundamentals." (n.d.). Correlated Solutions.

Baqersad, J., Poozesh, P., Niezrecki, C., Harvey, E., and Yarala, R. (2014). "Full Field Inspection of a Utility Scale Wind Turbine Blade Using Digital Image Correlation."

"Bridges." (2017). *ASCE's 2017 Infrastructure Report Card*.

"Correlated Solutions - Applications." (n.d.). *Digital Image Correlation Applications by Industry*.

"Correlated Solutions – Calibration." (n.d.).

"Correlated Solutions – The DIC Speckle Kit." (n.d.). *VIC Speckle Pattern Application Kit*.

De Wilder, K., Lava, P., Debruyne, D., Wang, Y., De Roeck, G., and Vandewalle, L. (2015). "Experimental Investigation on the Shear Capacity of Prestressed Concrete Beams Using Digital Image Correlation." *Engineering Structures*, 82, 82–92.

Garcia-Palencia, A. J., Santini-Bell, E., Sipple, J. D., and Sanayei, M. (2015). "Structural Model Updating of an In-service Bridge Using Dynamic Data." *Structural Control and Health Monitoring*, 22(10), 1265–1281.

Gul, M. (2009). "Investigation of Damage Detection Methodologies For Structural Health Monitoring." University of Central Florida.

Gul, M., and Catbas, F. N. (2011). "Damage Assessment with Ambient Vibration Data Using a Novel Time Series Analysis Methodology." *Journal of Structural Engineering*, 137(12), 1518–1526.

Pan, B., Qian, K., Xie, H., and Asundi, A. (2009). “Two-Dimensional Digital Image Correlation for In-plane Displacement and Strain Measurement: A Review.” *Measurement Science and Technology*, 20(6), 062001.

Reagan, D., Sabato, A., and Niezrecki, C. (2018). “Feasibility of Using Digital Image Correlation for Unmanned Aerial Vehicle Structural Health Monitoring of Bridges.” *Structural Health Monitoring*, 17(5), 1056–1072.

Sanayei, M., Phelps, J. E., Sipple, J. D., Bell, E. S., and Brenner, B. R. (2012). “Instrumentation, Nondestructive Testing, and Finite-Element Model Updating for Bridge Evaluation Using Strain Measurements.” *Journal of Bridge Engineering*, 17(1), 130–138.

Sanayei, M., and Saletnik, M. J. (1996). “Parameter Estimation of Structures from Static Strain Measurements. I: Formulation.” *Journal of Structural Engineering*, 122(5), 555–562.

Shafiei Dizaji, M., Alipour, M., and Harris, D. K. (2018). “Leveraging Full-Field Measurement from 3D Digital Image Correlation for Structural Identification.” *Experimental Mechanics*, 58(7), 1049–1066.

Wang, W., Mottershead, J. E., Ihle, A., Siebert, T., and Reinhard Schubach, H. (2011a). “Finite Element Model Updating from Full-field Vibration Measurement using Digital Image Correlation.” *Journal of Sound and Vibration*, 330(8), 1599–1620.

Wang, W., Mottershead, J. E., Sebastian, C. M., Patterson, E. A., Siebert, T., Ihle, A., and Pipino, A. (2011b). “Image Analysis for Full-Field Displacement/Strain Data: Method and Applications.” *Applied Mechanics and Materials*, 70, 39–44.

Zhang, Z., and Aktan, A. E. (1997). “Different Levels of Modeling for the Purpose of Bridge Evaluation.” *Applied Acoustics*, 50(3), 189–204.

BIOGRAPHY

Nicole Nmair graduated with her Bachelor of Science degree in Civil and Infrastructure Engineering from George Mason University in 2016. Nicole currently works full time in the civil engineering industry as a Structural Engineer for the Federal Highway Administration.